Highly efficient CRISPR-mediated homologous recombination via NHEJ deficiency rather than HDR factors overexpression in *Populus*

Ali Movahedi[1§*], Hui Wei[1§], Zhong-Hua Chen[2], Weibo Sun[1], Jiaxin Zhang[3], Dawei Li[1], Liming Yang[1*], and Qiang Zhuge[1*]

[1] College of Biology and the Environment, Co-Innovation Center for Sustainable Forestry in Southern China, Key Laboratory of Forest Genetics & Biotechnology, Ministry of Education, Nanjing Forestry University, Nanjing 210037, China

[2] School of Science, Hawkesbury Institute for the Environment, Western Sydney University, Penrith, NSW 2751, Australia

[3] School of Food Science and Pharmaceutical Engineering, Nanjing Normal University, Nanjing 210046, China

[*]Correspondence should be addressed to Qiang Zhuge, Ali Movahedi, and Liming Yang: College of Biology and the Environment, Co-Innovation Center for Sustainable Forestry in Southern China, Key Laboratory of Forest Genetics & Biotechnology, Ministry of Education, Nanjing Forestry University, Nanjing 210037, China. E-mail: qzhuge@njfu.edu.cn; ali_movahedi@njfu.edu.cn; yangliming@njfu.edu.cn; Fax: +86 25 85428701

§ These authors are equally as the first author

Running title: Highly efficient homologous recombination via *XRCC4* deficiency in poplar

Abstract

- Efficient homology-directed DNA repair (HDR) is a vital difficulty confronting researchers to replace the target genome's desired fragment. In plants, scientists have performed meticulous investigations on herbal, crops, and citrus trees using HDR effector proteins, CtIP and MRE11, to obtain double-stranded breaks (DSBs) more precisely. Although HDR efficiency in plants previously has been reported, no record has been declared about HDR efficiency in woody perennial *Populus*.
- Here, we hypothesized that inhibition of non-homologous recombination cofactors XRCC4 and enhancing the HDR pathway activities enable us to improve the HDR efficiency. In this study, the *BleoR* gene was used to integrate into the interested site and generated transformants against Zeocin antibiotics. We designed plasmids, including different fusions of HDR proteins and, together with the *XRCC4* target. Furthermore, we showed that TaqMan real-time PCR could be a powerful tool to verify HDR efficiency
- We confirmed that both applying HDR proteins and *XRCC4* deficiency simultaneously could improve HDR efficiency, which showed about fiftyfold more, and decremented polymorphisms about sixfold less than no affecting HDR and NHEJ pathways. We developed a new recombinant poplar genome to generate stable lines resistant to the Zeocin antibiotic.

Keywords: CRISPR; XRCC4; Homologous recombination; BleoR; *Populus trichocarpa*

Introduction

The clustered regularly interspaced short palindromic repeat (CRISPR)/CRISPR-associated (Cas) protein system has been widely developed for DNA sequence manipulation in recent years. The efficient molecular scissors of the Cas9 system generate double-strand breaks (DSB), which consequently initiates endogenous repair machinery typically via either the error-prone non-homologous end joining (NHEJ) pathway or the donor-dependent homology-directed repair (HDR) pathway (Symington and Gautier, 2011). NHEJ repair can randomly lead to small deletions or insertions (indels) at the DSB area, which then shifts the reading frame, interferes with the gene function, and has shown a predominant pathway and occurs among the cell cycle widely (Panier and Boulton, 2014). The HDR is rare but powerful for sequence insertion and replacement if a homologous DNA substrate is available (Puchta, 2005). Up to date, many studies have been carried out to improve the genetic modification of crops by HDR. For instance, one study has been carried out to increase *ARGOS8* expression by replacing the GOS2 promoter via HDR to drive *ARGOS8* expression (Shi et al., 2017). Another report showed an enhancement in the efficiency of the insertion of the 35S promoter in upstream of the *ANT1* gene in tomato (Cermak et al., 2015). Many publications also report the successful generation of null mutations in woody species via the NHEJ pathway since the first implementation in poplar (Bewg et al., 2018; Zhou et al., 2015). However, precise gene targeting and replacement were only reported in model plants such as *Arabidopsis* (Schiml et al., 2014) and rice (Li et al., 2016). Still, no report shows highly efficient HDR happened in woody perennials.

Many attempts have been made to improve gene targeting efficacy and accuracy (Liu et al., 2019). Lu et al. (2020) recently used chemically modified donor DNA to promote heritable sequence insertion and replacement via NHEJ and HDR repair pathways. Both-end phosphorothioate-linkage and 5′-phosphorylation modification facilitated NHEJ insertion with lengths up to 2,049bp. Furthermore, a tandem repeat-HDRs system was optimized for base substitutions and in-locus tags (Lu, Tian et al., 2020). Though another biotechnology breakthrough on prime editor presented the success bases of insertion in rice (Lin et al., 2020; Tang et al., 2020), HDR-mediated precise gene targeting is a promising method for a long time.

Manipulation of the DSB repair pathway to improve HDR frequency is the most common method to enhance precise gene knock-in. One of the main difficulties in HDR efficiency is the limited delivery of donor DNA templates (DDTs) into the cell nucleus. Previous data indicated that it is necessary to increase the number of cells containing DDTs at S/G2 cell division phases to increase HDR efficiency (Yang et al., 2016). Several traditional strategies were applied to enrich the DDTs availability, such as offering sufficient DDTs via the particle bombardment replicons (Gil-Humanes et al., 2017; Wang et al., 2017), protoplasts (Svitashev et al., 2016), the geminiviral-based replication (Butler et al., 2016; Dahan-Meir et al., 2018; van Vu et al., 2020; Wang et al., 2017), and RNA transcription (Li et al., 2019b), but this still is one of the significant problems across woody plants genome. In this case and regarding the high and reliable stability of genes transmitted by *Agrobacterium* and widely use to transduce genes into woody plant cells (Movahedi et al., 2014; Movahedi et al., 2015), there few reports on enhancing the Agrobacteria method delivery to increase the efficiency of transferring DDT and, consequently, the recovery of DSBs as HDR in woody trees (Ali et al., 2020; An et al., 2020). Above all, manipulating the effectors involved in either NHEJ or HDR pathway was more straightforward. The positive effects of recombinant homologous factors and their impact on enhancing HDR efficiency in mammalians have already been reported. Cas9 integrates with MRE11, CtIP, and Rad51, Rad52, and promotes significant HDR efficiency in human cells and decreases NHEJ significantly, with at least a 2-fold increase in HDR and a 6-fold increase in HDR/NHEJ ratio (Tran et al., 2019). On the other hand, inhibition of DNA ligase IV (LIG4), Ku 70, and Ku 80, which are outwardly involved only in NHEJ and known as the most critical NHEJ factors, protect DSB from discrediting by forming one heterodimeric complex to bind tightly and load additional repair proteins such as DNA ligase IV (Friesner and Britt, 2003; Grawunder et al., 1998a; Maruyama et al., 2015; Pierce et al., 2001; Tran et al., 2019) and increase the HDR efficiency up to 19-fold (Tran et al., 2019). In *Arabidopsis*, mutated *Ku70* or *Lig4* enhanced the HDR-based genome targeting to 5~16-fold or 3~4-fold respectively (Qi et al., 2013).

XRCC4 is another critical NHEJ factor that has not yet been considered for its interference effect on HDR efficiency. XRCC4 is one cofactor of LIG4 to interact with KU 70 and KU 80 and ligate the DSB (Grawunder et al., 1998b). To date, there is no report on combining

HDR factors overexpressing, specially CtIP and MRE11, and NHEJ factors suppression, specially XRCC4, to promote the HDR pathway in woody plants. Programmable endonucleases affect DSBs at target positions in genomic DNA and create undesired breaks outside of on-target positions and create off-target mutations. Cleavage at off-target sites direct to chromosomal rearrangements, including translocations, insertions, and deletions, which happen in the interruption of regular gene expression and the activation of oncogenes (Li et al., 2019a). Today, scientists have realized that reducing off-target may allow efficient and accurate genome editing (Wu and Yin, 2019). For this why, the effect of off-targets on efficient, precise genome editing and ways to reduce their impacts has already been studied (Hajiahmadi et al., 2019; Li et al., 2019a; Wu and Yin, 2019).

In eukaryotic kingdoms, Mitogen-activated protein kinase (MAPK or MPK) signaling is broadly crossed. In plants, they may direct signal pathways to resist the impacts of drought, cold, salt, scratch, and mechanical damage(Chen et al., 2020). Moreover, scientists have shown that MAPKs direct cellular responses against heat shock, osmotic, and other environmental stresses (Mohanta et al., 2015). Sun et al. (2015) investigated and comprised the *MAPK* genes from Maize (*Zea mays*), poplar (*Populus trichocarpa*), Arabidopsis (*Arabidopsis thaliana*), tomato (*Solanum lycopersicum*), and rice (*Oryza sativa*) to show the similarity of motifs, genomic structures, and domains. These authors also proved that *MAPK* genes are preferentially expressed in reproductive tissues and organs besides their roles against abiotic stress and ABA signaling. In Arabidopsis, *MAPKK2* (*MKK2*) are transcriptional regulator genes stimulated by environmental stresses such as salinity and cold to promote plant protection (Teige et al., 2004). To date, and regarding the importance of the MAPK pathway, there is no report on applying CRISPR genome editing through all involved genes to enhance its impact in the mentioned above roles.

Here, we aimed to develop the CRISPR/Cas9-mediated knock-in system in poplar with a haploid chromosome of 19 via NHEJ cofactor (XRCC4) suppression and HDR effectors (MRE11 and CtIP) overexpression. Also, we used the optimized homologous arms 400 bp to enhance the HDR activities, and the concentration of DDT fragments to facilitate the DDT delivery. We selected mitogen-activated protein kinases (MAPKs) as a case study. We also achieved the

stable transformant lines resistant against zeocin antibiotic with similar behavior to wild types against salinity stresses.

Materials and Methods

Plant Transformation

We cultivated *P. trichocarpa* seedlings in a phytotron at 23±2°C under a 16/8 light/dark time (Movahedi et al., 2015). To generate transgenic lines, we used stems from four weeks old young clones and dipped them in the optimized of *Agrobacterium tumefaciens* stimulant and pathogenic suspension (OD_{600}: 2.5, 120 min, pH ~5, Acetosyringone (As): 200 µM) (Movahedi et al., 2014) for 5 min with gentle shaking and then transferred to the semi-solid woody plant medium (WPM) added with 0.05 mg/L Indole-3-butyric acid (IBA), 0.006 mg/L thidiazuron (TDZ), 200 µM As and 0.5% (w/v) agar. Afterward, the stimulated stems were incubated in the dark at 23°C for two days. The assumed transformants were then co-cultivated in selection media enriched with 0.1 mg/L IBA, 0.006 mg/L TDZ, 100 mg/L cefotaxime, 8 mg/L hygromycin, 50 mg/L Zeocin and 0.8% (w/v) agar. Two weeks later, buds were regenerated and then sub-cultured independently in media including 0.1 mg/L IBA, 0.001 mg/L TDZ, 100 mg/L cefotaxime, 8 mg/L hygromycin, 50 mg/L Zeocin and 0.8% (w/v) agar. After six weeks, buds with four to six small leaves were transferred to the MS media with 0.1 mg/L IBA, 200 mg/L cefotaxime, 70 mg/L Zeocin, and 0.8% (w/v) agar to root. Five lines were used for each experiment independently, and each line included about ten individuals.

Targets and protein detection

We decided to target the *MKK2* gene from *P. trichocarpa* (POPTR_0018s05420g; Chromosome 18) because of its vital role in transcriptional regulation against environmental stresses. Therefore, we used Uniprot (https://www.uniprot.org/) to download MKK2 protein and then used the BLAST database of the National Center for Biotechnology Information (NCBI) (https://blast.ncbi.nlm.nih.gov/) to download full DNA sequences and CDS. To detect targets, we used Geneious Prime® 2020.1.1 to analyze *MKK2* locus and detect targets compared to the whole genome of *P. trichocarpa*, which has been already downloaded from NCBI (Supplementary Table 1) (Doench et al., 2014; Hsu et al., 2013). Geneious Prime® also has been used to analyze the *XRCC4* (POPTR_0010s08650g, Chromosome 10) gene for knocking out. The

PAM motif target sequences were concerned with the exon 8 area from the *MKK2* and exon 1 area from the *XRCC4* genes. Furthermore, and to evaluate the effect of HDR proteins and also proper function of edited *MKK2* gene in transformants, we used Uniprot to use CtIP (POPTR_001G269700v3), MRE11 (POPTR_0001s41800g), BRCA1 (POPTR_0005s26150g), Rad50 (POPTR_0001s32760g), Rad51 (POPTR_0014s06360g), Lig4 (POPTR_0018s13870g).

MKK2 locus target oligo synthesis

We designed a pair of oligos (Supplementary Table 2; *MKK2* Oligo-F and -R) flanked by *Bsa*I adaptors. Synthesized oligos were then ligated into digested pRGEB31 vectors by *Bsa*I restriction enzyme (Xie and Yang, 2013) to construct pgRNA (Supplementary 1a). Afterward, we transferred all vectors into *E. coli* (DH5α) and propagated under normal conditions. Vectors were then extracted using the plasmid midi kit (Qiagen, USA) and confirmed by sanger sequencing (GenScript, Nanjing).

Construction of DDT and pDDT

To produce DDT (Supplementary1b), we designed five fragments, constructed and ligated them, respectively (Supplementary2a). To construct fragment one, the OsU3 promoter and gRNA scaffold were isolated from pRGEB31 (Supplementary Table 2, OS1-F and -R) flanked by *Hind*III and *BamH*I endonucleases. To increase the amount of DDT in the cell nucleus and improve HDR efficiency, we decided to use the cleavage property of Cas9 with designing two special gRNA targets 1 and -2 (No on- and -off-targets through whole poplar genome) besides DDT (Zhang et al., 2017) (Supplementary 1b). Thus, we designed special gRNA oligos (Sgo1-F and -R) (Supplementary 2a; Supplementary Table 2, special gRNA oligo1-F and -R) as the described details (Xie and Yang, 2013) to form special gRNA target1 (Sgt1) and to ligate into the fragment one. To construct fragment two, we isolated 5' homology arm (400 bp) sequences from *P. trichocarpa* genomic DNA (Supplementary Table 2, 5' Ho-F-1 and -R-1). Afterward, regular PCR was carried out using primers with the extensions of *BamH*I-special target1 (St1) and 39 bp from complemented 5' of fragment 3 (Supplementary Table 2, 5' Ho-F-2 and -R-2) (Supplementary 2a) to achieve component two.

To construct fragment three, we isolated the BleoR CDS from the PCR®-XL-Topo® vector (Supplementary Table 2, BleoR-1092F and -2276R). Then, the overlap-PCR was performed

(Supplementary Table 2, BP1,2,3-F and -R) using isolated BleoR CDS as the template to add the remained sequences from exon 8 and exon 9 to the 5' region of BleoR CDS and also 6XHis and PolyA tail to the 3' area of BleoR CDS (Supplementary 2a). We isolated a 3' homology arm (400 bp) (Supplementary Table 2, 3' Ho-F-1 and -R-1) from *P. trichocarpa* genomic DNA to assemble fragment four. Then, we performed PCR to extend 3' homology arm with 30 bp Poly-T and *Nco*I-special target2 (St2) sequences (Supplementary Table 2, Ho-F-2 and -R-2) (Supplementary 2a). Finally, we performed standard PCR to isolate the OsU3 promoter and gRNA scaffold from pRGEB31 (Supplementary Table 2, Os2-F and Os2-R). Moreover, we designed special gRNA oligos (Sgo2-F and -R) (Supplementary 2a; Supplementary Table 2, special gRNA oligo2-F and -R) again as the described details (Xie and Yang, 2013) to form special gRNA target2 (Sgt2) and to ligate into the fragment five.

To construct pDDT, we ligated fragments three and two using PCR (Supplementary 2b). For this, we designed a 39 bp overhang on fragment two that was complementary to the end of fragment three to form preliminary DDT (Supplementary 2b). In this PCR, we prepared a PCR reaction with 500 ng of each component. We used everything in PCR reaction except primers and then denatured fragments at 95 degrees for 5 minutes and allowed two annealing and extension cycles. We allowed PCR products to anneal at 68 degrees to avoid nonspecific hybridization amongst the long PCR products for 30 seconds and then extend for one minute at 74 degrees to have a double-stranded outcome. Then we added the primers to the distal ends of fragments two and three and performed one standard PCR. We purified PCR products and ligated them into the pEASY vector to sequence and confirm. Then we ligated the preliminary DDT product to fragment four as described before and formed secondary DDT products (Supplementary 2b). After sequencing and confirmation, we used the restriction cloning technique to ligate secondary DDT products to fragments one and four (Supplementary 2b) to achieve DDT products. Briefly, we incubated a reaction including 50 ng of each digested fragments, 10x T4 DNA ligase buffer 0.5 ul, T4 DNA ligase (NEB) 1 ul, and H2O to 5 ul at 25 degrees for 4 hours and transferred into *E. Coli* DH5α competent cells for sequencing and confirmation. Subsequently, we used the restriction cloning technique to merge the DDT product and pRGEB31 vector and form the pDDT vector (Supplementary 2b).

Synthesis of pgCtIP and pgMR

To design a fused CtIP and Cas9 cassette, we isolated the CaMV35S promoter, 3xFLAG, and Cas9 CDS from pRGEB31 (Supplementary 3a) using designed primers (Supplementary Table 2). In the next step, we obtained CtIP CDS using RT-PCR from the *Populus trichocarpa* genome (Supplementary 3a; Supplementary Table 2, CtIP-F and -R). The 3'UTR and PolyA fragments were isolated from the pCAG-T3-hCAS-pA plasmid (Supplementary 3a; Supplementary Table 2, PolyA-F and -R). To complete pgCtIP, we ligated CaMV35S and 3xFLAG fragments using restriction cloning and formed backbone 1 (Supplementary 4a). The isolated Cas9 and the obtained CtIP CDS were also ligated, applying restriction cloning to form the backbone 2 (Supplementary 4a). The backbones 1 and 2 were then ligated using *Hind*III restriction cloning to form backbone 3 (Supplementary 4a). In the next step, the resulted backbone 3 was ligated to the assembled 3'UTR-PolyA using *Stu*I restriction cloning to form the CtIP cassette (Supplementary 4a; Supplementary 5a). We used *Sda*I and *Pme*I restriction enzymes to restrict the cloning of the CtIP cassette and pRGEB31 and achieve the pgCtIP plasmid (Supplementary 4a; Supplementary 5a).

To construct a fusion of MRE11 and Cas9, we isolated CaMV35 promoter, 3xFLAG, Cas9, 3'UTR, and PolyA as same the previous steps (Supplementary 3b; Supplementary Table 2). The MRE11 CDS was obtained recruiting extracted total RNA from *Populus trichocarpa* genome and RT-PCR as mentioned above (Supplementary 3b; Supplementary Table 2, MRE-F and R). To complete pgMR, we ligated the isolated CaMV35S and 3xFLAG fragments concerning *Xho*I endonuclease to form backbone 1 (Supplementary 4b). On the other hand, we constructed backbone 2 using the isolated Cas9 and 3'UTR-PolyA fragments (Supplementary 4b). The backbone 1, backbone 2, and MRE11 CDS product were then merged concerning *Not*I and *Nde*I restriction cloning to form MR cassette (Supplementary 4b; Supplementary 5b). Afterward, we used restriction cloning with *Sda*I and *Pme*I to construct pgMR plasmid (Supplementary 4b; Supplementary 5b).

Synthesis of pgCtMR and pggCtMR

To construct the CtMR cassette, we prepared all the required fragments, as mentioned above (Supplementary 3c). Afterward, we merged the CaMV35S and 3xFLAG components

using *Xho*I restriction cloning to form backbone 1 (Supplementary 6a). We then ligated backbone 1 and the already obtained MRE11 CDS product (Supplementary Table 2, MRE-F and -R) using *Not*I restriction cloning to form backbone 2 (Supplementary 6a). On the other hand, the isolated Cas9 and the obtained RT-PCR product CtIP CDS were ligated using *BamH*I restriction cloning to form backbone 3 (Supplementary 6a). We then used backbone 3 and isolated 3'UTR-PolyA fragment to form backbone 4 (Supplementary 6a). Eventually, we cloned backbones 2 and 4 to construct the CtMR cassette (Supplementary 6a; Supplementary 5c) and thereupon implemented *Sda*I and *Pme*I restriction cloning to ligate CtMR cassettes into pRGEB31, forming pgCtMR plasmid (Supplementary 6a; Supplementary 5c). To target the *XRCC4* gene and *MKK2* simultaneously, we designed one cassette, including both *XRCC4*, by adding one CRISPR site (Located on 5' region of target CDS) to mutate *XRCC4* (Non-off-target site on whole poplar genome; Activity score: 0.415; Specificity score: 100%) (Doench et al., 2014; Hsu et al., 2013), and *MKK2* gRNAs. For this purpose, we used primers (Supplementary Table 2, XR-Cass1-F and -R) to isolate the OsU3 promoter and gRNA scaffold from the pRGEB31 vector and then used *MKK2* designed oligos (Supplementary Table 2, *MKK2* Oligo-F and -R) to ligate *MKK2* target duplex (Supplementary 3d). Besides, we used primers (Supplementary Table 2; XR-Cass2-F and -R) to isolate the OsU3 promoter and gRNA scaffold again. In this process, we applied *XRCC4* designed oligos (Supplementary Table 2; XRCC4-Oligo1 and -2) to ligate the *XRCC4* target duplex (Supplementary 3d). The achieved fragments were then cloned using *Kas*I restriction cloning to form *XRCC4*-Cassette (Backbone 1) (Supplementary 6b; Supplementary 5d). Afterward, the *XRCC4*-Cassette was cloned into pRGEB31 using *Hind*III and *Sda*I restriction cloning to form backbone 2 (Supplementary 6b). Finally, we used *Sda*I and *Pme*I restriction cloning to clone the CtMR cassette into the backbone 2, forming pggCtMR plasmid (Supplementary 6b; Supplementary 5d). We performed PCR, cloning into pEASY T3 vector, and DNA sequencing in all the above processes for confirming the right ligation.

RT-PCR, DNA sequencing, Southern blotting, and Western blotting

Total RNA (100 ng/ml) was extracted from young leaves of five weeks grown buds on Zeocin with TRIzol. We then carried out reverse transcription using total RNA and oligo-dT primers to synthesize the first cDNA strand (PrimeScript One-Step RT-PCR Kit Ver.2, Takara

Biotechnology, Dalian, China) according to the manufacturer's instructions. Afterward, we designed two RT-PCR for both investigations of right *MKK2* transcription and right happening HDR. The first RT-PCR was intended to isolate a 920 bp of *MKK2* CDS (Supplementary Table 2, RT-F and R), while the forward primer was designed from 5' region of exon 9 (15 bp) and 3' region of exon 8 (15 bp). This RT-PCR purpose was to show the precise attaching of exon 8 and 9 to direct the transcription of *MKK2* correctly. The second RT-PCR was performed to isolate a 413 bp of recombinant CDS (Supplementary Table 2, RT-F-107 and RT-R-519). The forward primer was designed from *BleoR*, and the reverse primer was designed from exon 7 of *MKK2*. The purpose of this RT-PCR was to show the explicit HDR happening through our experiments via transcription of single mRNA from *MKK2* and BleoR.

Genomic DNA was extracted from young leaves of five weeks grown buds on Zeocin, applying the DNeasy Plant Mini Kit (Qiagen, USA). The quality of the extracted genomic DNA (250–350 ng/µl) was determined by a BioDrop spectrophotometer (UK). To DNA sequencing, we carried out PCR using designed primers (Supplementary Table 2, MKK2-S-7F and MKK2-S-1139R), Easy Taq polymerase (TransGene Biotech), and 50 ng of extracted genomic DNA as a template. All desired bands were then cut off from gels, purified, and sent to the company for sequencing (GeneScript, Nanjing), alignment, and analysis (Supplementary 7-11). Southern blotting was performed to verify the integration of *BleoR* into the poplar genome. 500 ng of genomic DNA was cleaved with *BamH*I and *Hind*III at 37 °C for 4 h. The digested DNA was then used as a PCR template to label a 160 bp probe from integrated *BleoR* CDS into the genomic DNA (Supplementary Table 2; S-F and -R). In this step, we used the DIG (digoxigenin) reagent, according to the manufacturer's instruction (catalog number 11745832910; Roche, Basel, Switzerland). PCR product was then segregated on a 0.8% agarose gel. The separated fragments were shifted on a Hybond N+ nylon membrane (Amersham Biosciences BV, Eindhoven, The Netherlands).

For extraction of proteins, 150 mg fresh leaves of five weeks grown buds were milled in 500 µl extraction buffer (125 mM Tris, pH 6.8, 4 M Urea, 5% β -mercaptoethanol, 4% w/v SDS). The centrifuge was then performed at 13,000 rpm for 10 min, and the supernatant was obtained for gel analysis. The extracted protein was then boiled in loading buffer (24% w/v

329 glycerol, 100 mM Tris, a drop amount of Bromophenol Blue, 4% v/v β -mercaptoethanol, 8%
330 w/v SDS) for 10 min. The extracted protein was analyzed by SDS-PAGE and conceived using
331 Coomassie brilliant blue R-250 staining. After that, we carried out western blotting according to
332 Sambrook et al. (1989) using a rabbit anti-His polyclonal antibody developed in our laboratory
333 as the primary and peroxidase-conjugated goat antirabbit IgG (Zhongshan Biotechnique, Beijing,
334 China) as the secondary antibody.

335 **TaqMan real-time PCR**

336 To test the effect of designed parameters in all experiments on the proper integration of
337 exogenous *BleoR* with both homology arms, we decided to run the TaqMan assay applying dye
338 labels such as FAM and VIC adopting Applied Biosystem real-time PCR (Applied Biosystems,
339 USA). We used high quality extracted genomic DNA (Refer to the southern blotting) as the
340 template for running TaqMan real-time PCR. In this assay, two fluorescent FAM and VIC will
341 attach to the 5' region of the probe, while a non-fluorescent quencher (NFQ) binds to the 3'
342 region. Thus, we designed primers to probe two 150 bp fragments FAM1 (Supplementary 2,
343 FAM1-F and -R) and FAM2 (Supplementary 2, FAM2-F and -R). These primers were designed so
344 that FAM1 was able to probe 114 bp nucleotides from the 5' homology arm and 36 bp from
345 BleoR. Besides, FAM2 could probe 105 bp nucleotides from the 3' homology arm and 45 bp
346 from the BleoR (Supplementary 12). We also designed primers (Supplementary Table2, VIC-F,
347 and -R) to probe one 106 bp fragment VIC on the *actin* gene as the reference with a stable copy
348 number (Supplementary 12). All samples were analyzed in quadruplicate.

349 **Evaluation of HDR efficiency**

350 To evaluate the HDR efficiency, we decided to calculate and compare the ΔΔCt mean of
351 BleoR expression integrated into the poplar genome from all grown buds in five designed
352 experiments separately. In this step, we used the synthesized cDNA (Point to the RT-PCR
353 section) and designed primers (Supplementary Table 2, BleoR-52F and -151R) to carry out real-
354 time PCR. We used the Fast Start Universal SYBR Green Master (Rox; No. 04913914001: Roche,
355 USA) and performed three technical repeats for each event. Then, we used ANOVA-One way to
356 analyze the achieved mean data and compared.

RT-qPCR

We applied RT-qPCR using synthesized cDNA from grown buds on Zeocin (as mentioned above) as the template and designed primers (Supplementary Table2, RT-qPCR part) to investigate the expression of *BleoR* and *MKK2* genes and their impact on each other. We also explored our method's impact to develop HDR efficiency on HDR (CtIP, MRE11, BRCA1, Rad50, and Rad51) and NHEJ (Lig4, XRCC4) influential factors.

Functional analyses and phenotypic properties

Regarding the critical roles of MKK2 in plant protection against environmental stresses (Mohanta et al., 2015; Teige et al., 2004), and to confirm the correct HDR happened through recovered events, we decided to assess the functional analyzes of *MKK2* and phenotypic properties affected by salt stress and compare with WT. Recovered events were then planted on soil and transferred to the greenhouse. After two weeks of acclimation, we extracted total RNA from all transferred recovered events. Then, we irrigated all recovered events daily with 50 mM NaCl for one week. Some plants withered. Therefore, we extracted total RNA from survived events to perform RT-qPCR with triplicates for each event and analyzed their stem lengths (mm) and -diameter (mm) before and after salt stress.

Statistical analysis

All data were analyzed using ANOVA One-Way with Turkey means comparison calculated by OriginPro 2018 and Excel 2019 software (Microsoft, Redmond, WA, USA). Differences were analyzed statistically when the confidence intervals presented no overlap of the mean values with an error value of 0.05.

Results and Discussion

Despite extensive research on using factors included in homology-directed repair pathway to enhance HDR efficiency in plants (An et al., 2020; Gil-Humanes et al., 2017; Hummel et al., 2018; Li et al., 2015; Svitashev et al., 2015), no research has been reported using this system in haploid woody species such as poplar.

Strategies for target detection and HDR

The importance of *the MKK2* gene role in plant protection has been shown against salt (Chen et al., 2020) and low temperature (Gao et al., 2017). In this study, the *MKK2* gene was

386 targeted for integrating *BleoR* into the poplar genome by improving HDR efficiency with Zeocin
387 resistance (Figure 1a). Guide RNA was designed near the 3' UTR to avoid rendering the gene
388 expression denoting higher specificity and less off-target (Hsu *et al.*, 2013; Doench *et al.*, 2014).
389 We targeted a detected CRISPR site located on exon 8 with the highest activity score and no off-
390 target effects on CDS throughout the whole *P. trichocarpa* genome (Figure 1a and
391 Supplementary Table 1). Afterthought and regarding (Song and Stieger, 2017), we optimized
392 the lengths of homologous arms (data not shown) to apply 400 bp upstream and downstream
393 of the PAM site as the 5' and 3' homology arms, respectively (Figure 1b). Furthermore,
394 particular sequences instead of remained nucleotides from exon 8 (Leu-Ala-Thr-Leu-Lys-Thr-Cys)
395 and exon 9 (Val-Leu-Val-Lys-Met) were added to the end of the 5' homology arm
396 (Supplementary 1b). Then, 375 bp *BleoR* CDS, 18 bp 6xHis tag, and 30 bp Poly A were designed
397 to attach the DDT sequences.

398 The DDT cassette was ligated into the pRGEB31 vector containing the Cas9 expression
399 cassette to construct the pDDT. It is worth remarking that to improve the HDR efficiency, we
400 overexpressed HDR effectors CtIP and MRE11 (Tran et al., 2019) and mutated the HDR inhibitor
401 XRCC4 (Pierce et al., 2001) simultaneously in this research. We constructed multiple fusion
402 vectors, including Cas9 expression cassette, CtIP overexpression cassette, MRE11
403 overexpression cassette, and *XRCC4* mutative cassette, improving the efficiency
404 (Supplementary 5a-d).

405 In this study, and to expand the genome editing possible for woody plants, we applied
406 Agrobacterium to deliver the optimized CRISPR–Cas9 system into poplar stems and generate
407 stable transgenic poplars. Because (Yang et al., 2016) reported that the HDR efficiency is
408 directly related to the amount of DDT at S/G2 cell division phases, we used pathogenic
409 suspension with an OD_{600}=2.5 (~2×10^9 cell ml-1) and the ratio of 4:1 pDDT/pgRNA to increase
410 DDT fragments during S/G2 cell division (Tran et al., 2019) and to avoid off-target editing
411 caused by the extra accumulation of pgRNA (Hajiahmadi et al., 2019) (Figure 2a). Transformant
412 grown buds on zeocin were selected to analyze (Figure 2a).

413 According to figure 2b, we transferred pgRNA and pDDT into the explants via
414 experiment I (ExI). After that, we decided to design a plasmid that included a fused CtIP (Tran et

al., 2019) and Cas9 (pgCtIP) instead of pgRNA with a ratio of 4:1 pDDT/pgCtIP to promote HDR efficiency in poplars via experiment II (ExII) (Figure 2b). Only seventeen events were observed to be grown from a total of 42 regenerated buds. Also, only one recovered event was discerned after transferring on rooting media. In continuous and to investigate the effect of MRE11 (Tran et al., 2019) to improve HDR efficiency in poplars, we designed plasmid harboring a combined MRE11 and Cas9 (pgMR) instead of pgRNA with the same ratio of 4:1 pDDT/pgMR via experiment III (ExIII) (Figure 2b). In this experiment, we observed fifteen grown buds, and only one recovered edited event. Because our experiments did not show significant recovered events in overcoming NHEJ to integrate *BleoR*, we determined to design experiment IV (ExIV), including one plasmid harboring fused both MRE11 and CtIP with Cas9 (pgCtMR). Recovered events were increased insignificantly to four (Figure 2b). Therefore, we decided to target *XRCC4* as one key factor in the NHEJ pathway (Maruyama et al., 2015) besides CtIP and MRE11 overexpressing. For this purpose, we designed experiment V (ExV) using one plasmid harboring *XRCC4* gRNA and also fused both MRE11 and CtIP with Cas9 (pggCtMR). We tried to transfer this plasmid into the plant cells with the same ratio of 4:1 pDDT/pggCtMR. In this experiment, recovered events were shown increased surprisingly to twelve events from thirty-one grown buds on selection media (Figure 2b).

Transformants verification via Western blotting, RT-PCR, and Southern blotting

Several methods, such as western blotting, RT-PCR, and Southern blotting, were applied to verify the happened HDR in resistant transformants. Several methods, such as western blotting, RT-PCR, and Southern blotting, were applied to verify the happened HDR in resistant transformants. We decided to combine a 6XHis tag to the BleoR CDS (Figure 1b) to show the integration of *BleoR* and *MKK2* through target genomes using Western blotting. Through screening the western blotting of all transformants grown on zeocin, we detected no edited events in ExI, but one ExII event (II#29) showed a band of 54 KDa (Figure 3a), which might be the candidate for the successful integration of the BleoR (~13.7 KDa) fused by the MKK2 (~40.5 KDa) (Figure 3b). In continue and through ExIII events, we found only one event (III#6) with a band of 14 KDa (Figure 3a), and we deemed that only BleoR CDS was integrated completely and sudden mutations might knock out *MKK2* throughout exons7, 8, or 9 (Figure 3b). We then

screened ExIV events and found three events (IV#17, #54, and #68) with bands about 54 KDa, and one event (IV#90) about 14 KDa (Figure 3a). Surprisingly, we found ten events (V#21, #25, #29, #32, #39, #59, #73, #88, #91, and #94) with bands about 54 KDa within ExV, and two events (V#37, and #53) with bands about 14 kDa (Figure 3a).

We designed two RT-PCR assays to confirm the designed editions in transformed poplars. Considering the targeting of exon8 from *MKK2* (Figure 1b) in this study and then our attempts to repair the damaged area together with the integration of *the BleoR* gene, we decided to design the first RT-PCR experiment in such a way as to repair the infected area and reassure the correct *MKK2* gene expression in transformant poplars (Figure 3c and d). As expected, no bands were observed from ExI events. Three ExII events (#24, #29, and #35) and four ExIII events (#10, #23, #36, and #45) showed 920 bp bands (Figure 3e) respectively. Also, ExIV events (#9, #17, #39, #45, #54, #60, #68, #72, and #83) showed similar bands with WT. Surprisingly, twenty events of ExV exhibited the complete *MKK2* expression with similar bands with WT. Regarding the binding of MKK2 and BleoR in the target genome (Figure 1b) and verify that, and also according to the design of DDT to include the required nucleotides from exon7, we decided to design a second RT-PCR using pDDT as the positive control (Figure 3d). The second RT-PCR also revealed no desired 413 bp band through ExI events (Figure 3f). ExII events revealed only one 413 bp amplification (#29), but ExIII events revealed no desired band. We then considered ExIV and observed three events (#17, #54, and #68), while ExV revealed significantly increased ten events (#21, #25, #29, #32, #39, #59, #73, #88, #91, and #94) as 413 bp bands. All events showing bands with Western blotting and RT-PCR assays were selected for further analyses. The probe of *BleoR* sequences was designed for Southern blotting (Figure 3g). Several events (III#6, IV#90, V#37, and V#53), which were not amplified through the second RT-PCR, were reverified in Southern blotting.

Accurate investigation of edited events and HDR efficiency

Cermak et al. (2015) could improve the HDR efficiency by ten-fold in tomato and integrated the 35S promoter in upstream of the *ANT1* gene. Tran et al. (2019) could promote the HDR efficiency in mammalians with at least a 2-fold increase in HDR and a 6-fold increase in HDR/NHEJ ratio. Aslan et al. (2017) increased HDR efficiency to 25.7% in the *Xenopus*

tropicalis genome by inserting mall pieces of DNA, while Danilo et al. (2018) succeeded in knocking in a DDT with 400 bp into the tomato genome with low efficiency of 1.29%. Jang et al. (2018) attempted to develop HDR efficiency to 38% in mouse lines by applying multiple sgRNAs, and Menchaca et al. (2020) tried to enhance the HDR efficiency to 61.5% in sheep utilizing single strand oligodeoxynucleotides. Still, there are some reports on *Populus* genome editing, but they are limited only to knock out genes, and mutations happened by Cas9 and Cas12a (An et al., 2020; Di Fan et al., 2015; Liu et al., 2015), but no report has been carried out on improving the HDR efficiency in poplar. In this study, we tried to create a recombinant genome in poplars using an HDR system. We then tried to detect the actual HDR events via TaqMan real-time PCR.

Two probes, FAM1 and FAM2, were designed for the 3' and 5'-end *BleoR* CDS area (Figure 4a). The transformants were assumed to be edited via exhibiting both fluorescent signals of FAM1 and FAM2 (Figure 4b). In ExI, the averages of fluorescent signals of FAM1 ΔΔCt and FAM2 ΔΔCt were shown proximal to 0 (Supplementary 13a). Most signals of ExI events exhibited as the mutant or WT, with a few partial FAM1 or FAM2 fluorescence (Figure 4c). Sanger sequencing was conducted to confirm these results. So, no edited events were achieved through ExI (Supplementary 7). Transformants of ExII and -III showed an increase in the signal densities of the FAM1 and FAM2 (Figure 4d, and e). The signal average of ExII transformants were about 14.5 and 13.5, while ExIII events exhibited more FAM1 ΔΔCt about 16 and a lesser FAM2 ΔΔCt about 10 (Supplementary 13b, and c). The alignment of Sanger sequencing well conformed to this result. In ExII, we found four fully edited events (II#7, II#19, II#53, and II#59), four FAM1 partial edited events (II#13, II#21, II#35, and II#41), and four FAM2 partial edited events (II#3, II#11, II#14, and II#23) (Supplementary 8; Supplementary 14a). In ExIII, we verified three fully edited events (III#21, III#45, and III#61), five FAM1 partial edited events (III#10, III#23, III#27, III#32, and III#53), and three FAM2 partial edited events (III#6, III17, and III#36) (Supplementary 9; Supplementary 14b). In ExIV, the signal density of edited events increased significantly (Figure 4f). The mean fluorescent signals of FAM1 ΔΔCt and FAM2 ΔΔCt showed an increase of about 19 and 15, respectively (Supplementary 13d). In total, nine fully edited events (IV#9, IV#27, IV#39, IV#45, IV#54, IV#68, IV#79, IV#83, and IV#90), seven FAM1 partial edited

events (IV#13, IV#17, IV#19, IV#46, IV#60, IV#75, and IV#85), and four FAM2 partial edited events (IV#13, IV#76, IV#80, and IV#92) (Supplementary 10; Supplementary 14c) were detected. Finally, the signal density of edited transformants in ExV was remarkably increased (Figure 4g). The mean fluorescent signals of FAM1 ΔΔCt and FAM2 ΔΔCt were increased about 21.5 and 18, respectively (Supplementary 13e). In total, 15 fully edited events (V#3, V#9, V#21, V#25, V#29, V#33, V#39, V#67, V#73, V#79, V#88, V#91, V#92, V#94, and V#101) were discovered (Supplementary 11; Supplementary 14d; Supplementary 17). Total FAM fluorescent signals (FAM1, FAM2, and FAM1&2) indicated the promotion of happened HDR through experiment events (Figure 4h). Overexpression of HDR effectors, CtIP, and MRE11 (ExIV), could dramatically increase FAM signals in comparison with the only overexpression of CtIP (ExII) or MRE11 (ExIII). Moreover, *XRCC4* deficiency, simultaneously with the overexpression of CtIP and MRE11, dramatically improved the HDR in ExV.

According to (Shao et al., 2017), improving the HDR factors causes to improve HDR efficiency. Tran et al. (2019) could improve the HDR efficiency up to 19-fold with overexpressing CtIP and MRE11 and inhibiting NHEJ factors (Li et al., 2018). In this study, we considered inhibiting XRCC4 as one LIG4 cofactor (Grawunder et al., 1998b) to increase HDR efficiency. The HDR efficiency investigation confirmed that the NHEJ pathway deficiency is meaningfully more efficient to HDR development than on only the overexpression of HDR factors (Figure 4i). Overexpression of CtIP, and MRE11, could dramatically increase FAM signals compared to the only overexpression of CtIP or MRE11. Furthermore, *XRCC4* deficiency, together with the overexpression of CtIP and MRE11, dramatically enhanced the HDR in ExV. According to Figure 4i, the expression of integrated exogenous *BleoR* represents HDR efficiency. We performed real-time PCR to evaluate the percentage of *BleoR* expression $\Delta\Delta C_t$ mean (Supplementary 15a) and then compare and illustrate the bar plot supported by standard distribution curves (Figure 4i; Supplementary 15b). The *BleoR* expression increased from -1.2287 in ExI to 4.40787 (5.6%) in ExII and 6.11543 (7.3%) in ExIII. The expression in ExIV and ExV raised to 19.06057 (20.26%) and 48.90032 (50.1%). We resulted that the *XRCC4* deficiency, together with the overexpression of CtIP and MRE11, was the most efficient system for HDR-based integration and improved more HDR happenings than the expression of HDR effectors CtIP and MRE11

(Figure 4i). We resulted that the *XRCC4* deficiency, together with the overexpression of CtIP and MRE11, was the most efficient system for HDR-based integration and improved more HDR happenings than the expression of HDR effectors CtIP and MRE11.

The effect of efficient HDR on the expression of NHEJ and HDR factors

It is required to investigate targeted *MKK2* and integrated *BleoR* gene expressions and their interdependence. The expression of each of them proves the HDR happening and shows the regular functions of these genes in the new version of the poplar genome. We analyzed RT-qPCR achieved data and used Violon plots to describe the distributed expressions of *MKK2* and *BleoR* genes through all events (Figure 5a-d) and Column plots to show their expressions for each event separately (Supplementary 16). Analysis among ExI events revealed distributed *MKK2* and *BleoR* expressions of about +1 and -1 but, the ExII events exhibited above expressions between about 100 and zero with medians about zero (Figure 5a and b). Within the ExII, we discovered three events with *MKK2* expression (#21, #29, and #35) and only one event with *BleoR* expression (#29) (Supplementary 16). We then analyzed these gene expressions from ExIII and discovered promoted distributed expressions of *MKK2* (Figure 5c). In this experiment, we found four events with *MKK2* expression (#10, #23, #36, and #45) and one event with *BleoR* expression (#6) (Supplementary 16). RT-qPCR results through ExV events revealed enhanced distributions of *BleoR* and *MKK2* expressions (Figure 5d). In this experiment, we achieved nine events with *MKK2* expression (#9, #17, #39, #45, #54, #60, #68, #79, and #83) and four events with *BleoR* expression (#17, #54, #68, and #90) (Supplementary 16). Regarding the expressions of these genes from ExV events, we observed significant promotions in *MKK2* and *BleoR* distributed expressions with a median of about 100 (Figure 5e). Also, the column bar analysis confirmed these distributions with twenty *MKK2* expressions within ExV events (#3, #9, #18, #21, #25, #29, #32, #33, #39, #59, #67, #73, #79, #82, #86, #88, #91, #92, #94, and #101) and twelve *BleoR* expressions (#21, #25, #29, #32, #37, #39, #53, #59, #73, #88, #91, and #94) (Supplementary 16).

Moreover, we decided to assess gene expressions involved in HDR and NHEJ pathways affected by our increasing HDR efficiency plans. We used a Heat-map plot to interpret the obtained data from RT-qPCR (Figure 5f). While the expressions

of *CtIP* (~116%), *MRE11* (~115%), *BRCA1* (~114%), *Rad50* (~113%), and *Rad51* (~116%) were increased through ExI compared to WT, more expressions were observed in *Lig4* (~146%) and *XRCC4* (~143%) (Figure 5f). The expression of *CtIP* was increased impressively (~166%) via ExII compared with WT, while the expressions of *MRE11* (~129%), *BRCA1* (~119%), *Rad50* (~120%), and *Rad51* (~121%) were increased insignificantly. Through ExII, the expressions of *Lig4* (~104%) and *XRC44* (~105%) were decreased compared to ExI (Figure 5f). Within ExIII, the expression of *MRE11* was increased impressively (~162%), but the expressions of *CtIP* (~134%), *BRCA1* (~120%), *Rad50* (~122%), and *Rad51* (~119%) were increased slightly. Within this experiment, the expressions of *Lig4* (~107%) and *XRC44* (~103%) were decreased, contrasted with ExI (Figure 4f). All HDR factors revealed enhanced expressions among ExIV as *CtIP* (~165%), *MRE11* (~164%), *BRCA1* (~130%), *Rad50* (~128%), and *Rad51* (~129%), but the expressions of *Lig4* (~101%) and *XRC44* (~99%) were decreased more compared with ExI (Figure 5f). *XRCC4* deficiency in ExV and enhancing *CtIP* and *MRE11* expressions caused enhancing the expressions of *CtIP* (~170%) and *MRE11* (~165%) much more than WT events. Also, the expression of *Lig4* (~87%) revealed more decreased than WT, and *XRCC4* was knocked out. Through ExV, the other HDR factors *BRCA1* (~145%), *Rad50* (~139%), and *Rad51* (~142%) also revealed more expressions (Figure 5f).

XRCC4 deficient dramatically enhanced HDR efficiency and decreased polymorphisms

NHEJ is identified by introducing irregular small insertions or deletions (indels) into the targeted site. Notwithstanding the mutagenicity of NHEJ for its error-prone trait, its active kinetics has a role in repairing genome integrity, distinctly by crushing chromosomal translocations, mostly for the bulk of repair events (Ceccaldi et al., 2016). It has been exhibited a numerous percentage of about 70% of polymorphisms, especially deletions in Populus genome editing by the Cas system while knocking down the PDS gene family (An et al., 2020). Menchaca et al. (2020) recorded 17.8% indel mutations in sheep genome editing, with 61.5% knock-in mutations happened by HDR. Also, it has been shown that silencing of NHEJ factors such as *Ku70* and *Ku80* caused to reduce indels significantly from 64% to 38% and 39.4%, respectively (Li et al., 2018).

In this study, and to test whether the HDR promotion affects decreasing the polymorphisms, we analyzed the variant genotypes, protein effects, and nucleotide genotyping within the 5' and 3' homologous arms and also the knocked-in fragments from recovered events. We firstly analyzed the homology arms to detect polymorphisms and detected seven polymorphism varieties, including deletions, deletion tandem repeats, insertions, insertion tandem repeats, SNP transitions (A to C or G to T and reversely), SNP transversions (Purines to pyrimidines or reversely), and substitutions (Supplementary Table 3). It has been shown that the promotion of HDR via ExI to ExV events push to migrate Insertion and Deletion (InDel) nucleotides from the 5' region of knocked-in fragments (BleoR) to the 3' region (6xHis and PolyA) (Figure 6a). It means that we achieved more *BleoR* expression via ExV events compared to the other experiments. The mean comparisons of the InDel nucleotides revealed that the promoted HDR by *XRCC4* deficiency caused to decrease in InDel nucleotides considerably via ExV events (65) compared to the ExI (454), ExII (263), ExIII (177), and ExIV events (295) (Figure 6b). We then calculated the only number of happened polymorphisms (Not nucleotides) and then compared the means obtained from the total polymorphisms issued within designed experiments. It has been observed that the HDR happening through ExI events provoked the highest polymorphisms, significantly more than ExIV and -V events (Figure 6c). We also observed more happened polymorphisms within ExII and -III than ExIV and -V (Figure 6c). We then decided to investigate all happened polymorphisms in more detail from the homology arms and knocked-in *BleoR* from the recovered poplar genome (Supplementary Table 4). We identified the highest frequency of deletions through ExI events and the least within ExV events (Figure 6d). We also observed that *XRCC4* deficiency revealed the least of SNP transition. The overexpression of *CtIP* decremented deletion tandem repeats (ExII), and the overexpression of *MRE11* decremented SNPs, SNP transitions, and SNP transversions (Figure 6d). The overexpression of *CtIP* and *MRE11* simultaneously (ExIV) decremented substitution polymorphisms (Figure 6d). Moreover, the whisker plot of total polymorphisms presented the maximum distribution of polymorphisms through ExI events and the minimum of those in ExV events (Figure 6d).

Functional analyzes of MKK2 and phenotypic changes

It has been shown that MAPKs genes direct cellular responses against abiotic stresses such as salinity (Mohanta et al., 2015; Sun et al., 2015). Regarding these results, we decided to evaluate *MKK2* expression from re-planted recovered events on the soil before and after salt stress to show the proper *MKK2* locus maintain by efficient HDR through exon7, 8, and 9. The functional analysis of *MKK2* in survived recovered events (II#29, IV#17, IV#54, IV#68, V#21, V#25, V#29, V#32, V#39, V#59, V#73, V#88, V#91, and V#94) from ExII, -IV and -V and comparing them with WT poplars revealed a regular expression in all events (~95%-100%) before stress and a stable overexpression induced by salt (168%-173%) after stress (Figure 7; Supplementary Table 5). Also, stem lengths and diameters of all mentioned above events before and after salt stress were measured and revealed no significant differences between survived recovered events and WT poplars (Figure 7; Supplementary Table 5).

In summary, we have proved that *XRCC4* deficiency caused to enhance the HDR efficiency meaningfully, therefore greatly expanding our capacity to improve hereditary developments in poplar. This breakthrough technology is likely to encourage biotechnological researches, breeding programs, and forest conservation of tree species.

Supplementary information

Supplemental information is available for this paper.

Funding

This project was funded by the National Key Program on Transgenic Research (2018ZX08020002), the National Natural Science Foundation of China (No. 31971682, 31570650), the Priority Academic Program Development of Jiangsu Higher Education Institutions, the Talent Funding Project of Nanjing Forestry University (No. 163108059).

Author contribution

AM: Conceptualization, Software, Formal analysis, Writing - Original Draft, Visualization, Project administration, and Funding acquisition; HW: Methodology, Formal analysis, Writing - Review & Editing and Data Curation; ZHC: Conceptualization, Validation, Data Curation, Writing - Review & Editing; WS, JZ, DL: Validation, Writing - Review & Editing; LY: Conceptualization,

Software, Formal analysis, Visualization, and Funding acquisition; QZ: Conceptualization, Software, Formal analysis, Visualization, Supervision, and Funding acquisition.

Conflict of interest

The authors declare that they have no conflict of interest.

Acknowledgment

We thank all researchers, especially professor Zhong-Hua Chen, to improve this research with their directions.

References

Ali, Z., Shami, A., Sedeek, K., Kamel, R., Alhabsi, A., Tehseen, M., Hassan, N., Butt, H., Kababji, A., Hamdan, S. M. and Mahfouz, M. M. (2020) Fusion of the Cas9 endonuclease and the VirD2 relaxase facilitates homology-directed repair for precise genome engineering in rice. *Commun Biol* **3**.

An, Y., Geng, Y., Yao, J., Fu, C., Lu, M., Wang, C. and Du, J. (2020) Efficient Genome Editing in Populus Using CRISPR/Cas12a. *Front Plant Sci* **11**, 593938.

Aslan, Y., Tadjuidje, E., Zorn, A. M. and Cha, S. W. (2017) High-efficiency non-mosaic CRISPR-mediated knock-in and indel mutation in F0 Xenopus. *Development* **144**, 2852–2858.

Bewg, W. P., Ci, D. and Tsai, C.-J. (2018) Genome Editing in Trees: From Multiple Repair Pathways to Long-Term Stability. *Frontiers in Plant Science* **9**.

Butler, N. M., Baltes, N. J., Voytas, D. F. and Douches, D. S. (2016) Geminivirus-Mediated Genome Editing in Potato (Solanum tuberosum L.) Using Sequence-Specific Nucleases. *Front Plant Sci* **7**, 1045.

Ceccaldi, R., Rondinelli, B. and D'Andrea, A. D. (2016) Repair Pathway Choices and Consequences at the Double-Strand Break. *Trends in cell biology* **26**, 52–64.

Cermak, T., Baltes, N. J., Cegan, R., Zhang, Y. and Voytas, D. F. (2015) High-frequency, precise modification of the tomato genome. *Genome Biol* **16**, 232.

Chen, X. Y., Wang, P. K., Zhao, F. F., Lu, L., Long, X. F., Hao, Z. D., Shi, J. S. and Chen, J. H. (2020) The Liriodendron chinense MKK2 Gene Enhances Arabidopsis thaliana Salt Resistance. *Forests* **11**.

674 Dahan-Meir, T., Filler-Hayut, S., Melamed-Bessudo, C., Bocobza, S., Czosnek, H., Aharoni, A.,
675 and Levy, A. A. (2018) Efficient in planta gene targeting in tomato using geminiviral
676 replicons and the CRISPR/Cas9 system. *Plant J* **95**, 5–16.
677 Danilo, B., Perrot, L., Botton, E., Nogue, F. and Mazier, M. (2018) The DFR locus: A smart
678 landing pad for targeted transgene insertion in tomato. *Plos One* **13**.
679 Di Fan, Liu, T., Li, C., Jiao, B., Li, S., Hou, Y. and Luo, K. (2015) Efficient CRISPR/Cas9-
680 mediated Targeted Mutagenesis in Populus in the First Generation. *Sci Rep-Uk* **5**, 12217.
681 Doench, J. G., Hartenian, E., Graham, D. B., Tothova, Z., Hegde, M., Smith, I., Sullender, M.,
682 Ebert, B. L., Xavier, R. J. and Root, D. E. (2014) Rational design of highly active sgRNAs
683 for CRISPR-Cas9-mediated gene inactivation. *Nat Biotechnol* **32**, 1262–1267.
684 Friesner, J. and Britt, A. B. (2003) Ku80- and DNA ligase IV-deficient plants are sensitive to
685 ionizing radiation and defective in T-DNA integration. *Plant J* **34**, 427–440.
686 Gao, J., Zhang, S., He, W. D., Shao, X. H., Li, C. Y., Wei, Y. R., Deng, G. M., Kuang, R. B., Hu,
687 C. H., Yi, G. J. and Yang, Q. S. (2017) Comparative Phosphoproteomics Reveals an
688 Important Role of MKK2 in Banana (Musa spp.) Cold Signal Network. *Sci Rep-Uk* **7**.
689 Gil-Humanes, J., Wang, Y., Liang, Z., Shan, Q., Ozuna, C. V., Sanchez-Leon, S., Baltes, N. J.,
690 Starker, C., Barro, F., Gao, C. and Voytas, D. F. (2017) High-efficiency gene targeting in
691 hexaploid wheat using DNA replicons and CRISPR/Cas9. *Plant J* **89**, 1251–1262.
692 Grawunder, U., Zimmer, D., Fugmann, S., Schwarz, K. and Lieber, M. R. (1998a) DNA ligase
693 IV is essential for V(D)J recombination and DNA double-strand break repair in human
694 precursor lymphocytes. *Mol Cell* **2**, 477–484.
695 Grawunder, U., Zimmer, D., Kulesza, P., and Lieber, M. R. (1998b) Requirement for an
696 interaction of XRCC4 with DNA ligase IV for wild-type V(D)J recombination and DNA
697 double-strand break repair in vivo. *J Biol Chem* **273**, 24708–24714.
698 Hajiahmadi, Z., Movahedi, A., Wei, H., Li, D. W., Orooji, Y., Ruan, H. H. and Zhuge, Q. (2019)
699 Strategies to Increase On-Target and Reduce Off-Target Effects of the CRISPR/Cas9 System
700 in Plants. *Int J Mol Sci* **20**.
701 Hsu, P. D., Scott, D. A., Weinstein, J. A., Ran, F. A., Konermann, S., Agarwala, V., Li, Y., Fine,
702 E. J., Wu, X., Shalem, O., Cradick, T. J., Marraffini, L. A., Bao, G. and Zhang, F. (2013)
703 DNA targeting specificity of RNA-guided Cas9 nucleases. *Nat Biotechnol* **31**, 827–832.

Hummel, A. W., Chauhan, R. D., Cermak, T., Mutka, A. M., Vijayaraghavan, A., Boyher, A., Starker, C. G., Bart, R., Voytas, D. F. and Taylor, N. J. (2018) Allele exchange at the EPSPS locus confers glyphosate tolerance in cassava. *Plant Biotechnol J* **16**, 1275–1282.

Jang, D. E., Lee, J. Y., Lee, J. H., Koo, O. J., Bae, H. S., Jung, M. H., Bae, J. H., Hwang, W. S., Chang, Y. J., Lee, Y. H., Lee, H. W. and Yeom, S. C. (2018) Multiple sgRNAs with overlapping sequences enhance CRISPR/Cas9-mediated knock-in efficiency. *Exp Mol Med* **50**.

Li, G. L., Liu, D. W., Zhang, X. W., Quan, R., Zhong, C. L., Mo, J. X., Huang, Y. Q., Wang, H. Q., Ruan, X. F., Xu, Z., Zheng, E. Q., Gu, T., Hong, L. J., Li, Z. C., Wu, Z. F., and Yang, H. Q. (2018) Suppressing Ku70/Ku80 expression elevates homology-directed repair efficiency in primary fibroblasts. *Int J Biochem Cell B* **99**, 154–160.

Li, J., Hong, S., Chen, W., Zuo, E. and Yang, H. (2019a) Advances in detecting and reducing off-target effects generated by CRISPR-mediated genome editing. *J Genet Genomics*.

Li, J., Meng, X., Zong, Y., Chen, K., Zhang, H., Liu, J. and Gao, C. (2016) Gene replacements and insertions in rice by intron targeting using CRISPR-Cas9. *Nat Plants* **2**, 16139.

Li, S., Li, J., He, Y., Xu, M., Zhang, J., Du, W., Zhao, Y. and Xia, L. (2019b) Precise gene replacement in rice by RNA transcript-templated homologous recombination. *Nat Biotechnol* **37**, 445–450.

Li, Z., Liu, Z. B., Xing, A., Moon, B. P., Koellhoffer, J. P., Huang, L., Ward, R. T., Clifton, E., Falco, S. C., and Cigan, A. M. (2015) Cas9-Guide RNA Directed Genome Editing in Soybean. *Plant Physiol* **169**, 960–970.

Lin, Q., Zong, Y., Xue, C., Wang, S., Jin, S., Zhu, Z., Wang, Y., Anzalone, A. V., Raguram, A., Doman, J. L., Liu, D. R. and Gao, C. (2020) Prime genome editing in rice and wheat. *Nat Biotechnol* **38**, 582–585.

Liu, M., Rehman, S., Tang, X., Gu, K., Fan, Q., Chen, D. and Ma, W. (2019) Methodologies for Improving HDR Efficiency. *Frontiers in Genetics* **9**.

Liu, T.-t., Di Fan, Ran, L.-y., Jiang, Y.-z., Liu, R. and Luo, K.-m. (2015) Highly efficient CRISPR/Cas9-mediated targeted mutagenesis of multiple genes in Populus. *Yi Chuan = Hereditas* **37**, 1044–1052.

733 Lu, Y., Tian, Y., Shen, R., Yao, Q., Wang, M., Chen, M., Dong, J., Zhang, T., Li, F., Lei, M. and
734 Zhu, J. K. (2020) Targeted, efficient sequence insertion and replacement in rice. *Nat*
735 *Biotechnol* **38**, 1402–1407.
736 Maruyama, T., Dougan, S. K., Truttmann, M. C., Bilate, A. M., Ingram, J. R. and Ploegh, H. L.
737 (2015) Increasing the efficiency of precise genome editing with CRISPR-Cas9 by inhibition
738 of non-homologous end joining. *Nat Biotechnol* **33**, 538–542.
739 Menchaca, A., dos Santos-Neto, P. C., Souza-Neves, M., Cuadro, F., Mulet, A. P., Tesson, L.,
740 Chenouard, V., Guiffes, A., Heslan, J. M., Gantier, M., Anegon, I. and Crispo, M. (2020)
741 Otoferlin gene editing in sheep via CRISPR-assisted ssODN-mediated Homology Directed
742 Repair. *Sci Rep-Uk* **10**.
743 Mohanta, T. K., Arora, P. K., Mohanta, N., Parida, P. and Bae, H. (2015) Identification of new
744 members of the MAPK gene family in plants shows diverse conserved domains and novel
745 activation loop variants. *BMC genomics* **16**, 58.
746 Movahedi, A., Zhang, J. X., Amirian, R. and Zhuge, Q. (2014) An Efficient Agrobacterium-
747 mediated Transformation System for Poplar. *Int J Mol Sci* **15**, 10780–10793.
748 Movahedi, A., Zhang, J. X., Gao, P. H., Yang, Y., Wang, L. K., Yin, T. M., Kadkhodaei, S.,
749 Ebrahimi, M. and Qiang, Z. G. (2015) Expression of the chickpea CarNAC3 gene enhances
750 salinity and drought tolerance in transgenic poplars. *Plant Cell Tiss Org* **120**, 141–154.
751 Panier, S. and Boulton, S. J. (2014) Double-strand break repair: 53BP1 comes into focus. *Nat*
752 *Rev Mol Cell Biol* **15**, 7–18.
753 Pierce, A. J., Hu, P., Han, M., Ellis, N. and Jasin, M. (2001) Ku DNA end-binding protein
754 modulates homologous repair of double-strand breaks in mammalian cells. *Genes Dev* **15**,
755 3237–3242.
756 Puchta, H. (2005) The repair of double-strand breaks in plants: mechanisms and consequences
757 for genome evolution. *J Exp Bot* **56**, 1–14.
758 Qi, Y., Zhang, Y., Zhang, F., Baller, J. A., Cleland, S. C., Ryu, Y., Starker, C. G. and Voytas, D.
759 F. (2013) Increasing frequencies of site-specific mutagenesis and gene targeting in
760 Arabidopsis by manipulating DNA repair pathways. *Genome Res* **23**, 547–554.
761 Sambrook, J., Fritsch, E.F. and Maniatis, T. (1989). *Molecular cloning: a laboratory manual*,
762 2nd edn. Cold Spring Harbor, NY: Cold Spring Harbor Laboratory Press.

763 Schiml, S., Fauser, F. and Puchta, H. (2014) The CRISPR/Cas system can be used as nuclease
764 for in planta gene targeting and as paired nickases for directed mutagenesis in Arabidopsis
765 resulting in heritable progeny. *Plant J* **80**, 1139–1150.
766 Shao, S. M., Ren, C. H., Liu, Z. T., Bai, Y. C., Chen, Z. L., Wei, Z. H., Wang, X., Zhang, Z. Y.
767 and Xu, K. (2017) Enhancing CRISPR/Cas9-mediated homology-directed repair in
768 mammalian cells by expressing Saccharomyces cerevisiae Rad52. *Int J Biochem Cell B* **92**,
769 43–52.
770 Shi, J., Gao, H., Wang, H., Lafitte, H. R., Archibald, R. L., Yang, M., Hakimi, S. M., Mo, H. and
771 Habben, J. E. (2017) ARGOS8 variants generated by CRISPR-Cas9 improve maize grain
772 yield under field drought stress conditions. *Plant Biotechnol J* **15**, 207–216.
773 Song, F. and Stieger, K. (2017) Optimizing the DNA Donor Template for Homology-Directed
774 Repair of Double-Strand Breaks. *Mol Ther Nucleic Acids* **7**, 53–60.
775 Sun, W., Chen, H., Wang, J., Sun, H. W., Yang, S. K., Sang, Y. L., Lu, X. B. and Xu, X. H.
776 (2015) Expression analysis of genes encoding mitogen-activated protein kinases in maize
777 provides a key link between abiotic stress signaling and plant reproduction. *Funct Integr*
778 *Genomic* **15**, 107–120.
779 Svitashev, S., Schwartz, C., Lenderts, B., Young, J. K. and Cigan, A. M. (2016) Genome editing
780 in maize directed by CRISPR-Cas9 ribonucleoprotein complexes. *Nat Commun* **7**.
781 Svitashev, S., Young, J. K., Schwartz, C., Gao, H., Falco, S. C. and Cigan, A. M. (2015)
782 Targeted Mutagenesis, Precise Gene Editing, and Site-Specific Gene Insertion in Maize
783 Using Cas9 and Guide RNA. *Plant Physiol* **169**, 931–945.
784 Symington, L. S., and Gautier, J. (2011) Double-strand break end resection and repair pathway
785 choice. *Annu Rev Genet* **45**, 247–271.
786 Tang, X., Sretenovic, S., Ren, Q., Jia, X., Li, M., Fan, T., Yin, D., Xiang, S., Guo, Y., Liu, L.,
787 Zheng, X., Qi, Y. and Zhang, Y. (2020) Plant Prime Editors Enable Precise Gene Editing in
788 Rice Cells. *Mol Plant* **13**, 667–670.
789 Teige, M., Scheikl, E., Eulgem, T., Dóczi, R., Ichimura, K., Shinozaki, K., Dangl, J. L., and Hirt,
790 H. (2004) The MKK2 pathway mediates cold and salt stress signaling in Arabidopsis. *Mol*
791 *Cell* **15**, 141–152.

792 Tran, N. T., Bashir, S., Li, X., Rossius, J., Chu, V. T., Rajewsky, K. and Kuhn, R. (2019)
793 Enhancement of Precise Gene Editing by the Association of Cas9 With Homologous
794 Recombination Factors. *Front Genet* **10**.
795 Van Vu, T., Sivankalyani, V., Kim, E.-J., Doan, D. T. H., Tran, M. T., Kim, J., Sung, Y. W.,
796 Park, M., Kang, Y. J. and Kim, J.-Y. (2020) Highly efficient homology-directed repair using
797 CRISPR/Cpf1-geminiviral replicon in tomato. *Plant Biotechnol J*.
798 Wang, M. G., Lu, Y. M., Botella, J. R., Mao, Y. F., Hua, K. and Zhu, J. K. (2017) Gene
799 Targeting by Homology-Directed Repair in Rice Using a Geminivirus-Based CRISPR/Cas9
800 System. *Mol Plant* **10**, 1007–1010.
801 Wu, J., and Yin, H. (2019) Engineering guide RNA to reduce the off-target effects of CRISPR. *J*
802 *Genet Genomics*.
803 Xie, K. B., and Yang, Y. N. (2013) RNA-Guided Genome Editing in Plants Using a CRISPR-
804 Cas System. *Mol Plant* **6**, 1975–1983.
805 Yang, D., Scavuzzo, M. A., Chmielowiec, J., Sharp, R., Bajic, A. and Borowiak, M. (2016)
806 Enrichment of G2/M cell cycle phase in human pluripotent stem cells enhances HDR-
807 mediated gene repair with customizable endonucleases. *Sci Rep* **6**, 21264.
808 Zhang, J. P., Li, X. L., Li, G. H., Chen, W., Arakaki, C., Botimer, G. D., Baylink, D., Zhang, L.,
809 Wen, W., Fu, Y. W., Xu, J., Chun, N., Yuan, W., Cheng, T. and Zhang, X. B. (2017)
810 Efficient precise knockin with a double cut HDR donor after CRISPR/Cas9-mediated double-
811 stranded DNA cleavage. *Genome Biol* **18**, 35.
812 Zhou, X., Jacobs, T. B., Xue, L. ‐ J., Harding, S. A. and Tsai, C. ‐ J. (2015) Exploiting SNP s for
813 biallelic CRISPR mutations in the outcrossing woody perennial *Populus* reveals 4 ‐
814 coumarate: CoA ligase specificity and redundancy. *New Phytologist* **208**, 298–301.

815 **Figure legends**

816 **Figure 1:** Schematics of *MKK2* locus before and after edition and integrating exogenous
817 *BleoR* CDS into the poplar genome. **(a)** Schematic of this research purpose to integrate
818 exogenous BleoR into the poplar genome. Dash line reveals the target site. **(b)** Protospacer
819 Adjacent Motif (PAM) was detected at the end of exon 8 to lead Cas9. 400 bp sequences from
820 both sides of the CRISPR target were selected for HDR in this study. The 5' homology arm
821 included part sequences of the intron between exon 6 and -7, exon 7, intron sequences

between exon 7 and -8, and a part of exon 8. The 3' homology arm included intron sequences between exon 8 and -9 and 3' UTR of the *MKK2* locus up to 400 bp. Designed DDT included remained sequences of exon 8, exon 9, BleoR CDS, 6xHis, and PolyA sequences flanked by the 3'- and 5' homology arms. We added two special targets besides DDT. The DDT was then ligated into the pRGEB31 vector to form pDDT.

Figure 2: The transformation strategy and designing of experiments. **(a)** pDDT and pgRNA were mixed 4:1 and introduced to the Agrobacterium tumefaciens to form inoculator suspension. We condensed the inoculator up to OD_{600}=2.5 and then dipped all cut off stems. The putatively edited events were regenerated on Zeocin. We allowed putative edited events to bud. The grown buds were then transferred on selective rooting media and allowed to be recovered. Recovered events were then planted on soil and following two weeks of acclimation introduced by salt stress. **(b)** Designed experiments for this study including (I) No HDR factors, (II) overloaded CtIP, (III) overloaded MRE11, (IV) Overloaded CtIP+MRE11, and (V) Overloaded CtIP+MRE11 with *XRCC4* deficiency.

Figure 3: Western blotting to reveal the fused 6xHis tag with BleoR integration into the poplar genome. **(a)** Different experiments exhibited different quantities of 6xHis tag fusion. **(b)** Schematic of fusion 6xHis tag with edited poplar genome triggered by different experiments. Shape 1 reveals successful fusion of *BleoR* and *MKK2* with about 54 kDa. Shape 2 reveals an unsuccessful combination of mentioned proteins with about 14 kDa. **(c)** Schematic of right HDR happening caused to attach exon 8 and 9 in the edited genome. **(d)** Schematic of proper integration in edited genome caused to connect the BleoR to the C-terminal of MKK2. **(e)** RT-PCR exhibited the HDR in exon 8 and 9, revealing a 920 bp of transcribed *MKK2* RNA in triggered events from ExII to ExV. The β-actin was used as the control in all RT-PCR assays; WT was positive. **(f)** RT-PCR revealed that BleoR CDS was adequately inserted in the target region with amplifying 413 bp of transcribed RNA in the recovered events. The *β-actin* was used as the control in all RT-PCR assays; BleoR protein extracted from pDDT plasmid was used as the positive control. WT was used as the negative control. **(g)** Schematic of probing BleoR in edited events and WT as the control using Southern blotting. **(h)** Southern blot proved that *BleoR* CDS

was integrated into the precise recombinant genome. Digested pDDT plasmid was used as the positive control.

Figure 4: The 2D kernel density plot of TaqMan real-time PCR fluorescent intensities and HDR efficiency percentage. **(a)** The TaqMan real-time PCR assay designing to detect HDR happened, and evaluation included FAM1 and FAM2 DNA binding probes. **(b)** Strategy to classify edited events. **(c)** Experiment I revealed no density for the edited events. **(d)** The density plot of FAM1 and -2 intensities resulted from experiment II revealed an expansion in edited events against partial, mutant, and wild-types. **(e)** The density plot of FAM1 and -2 ΔΔCt resulted from experiment III revealed an increased intensity of partial FAM1 events. **(f)** Experiment IV revealed a remarkable increase of edited events signals in confronting with three earlier experiments. **(g)** The Density plot of experiment V revealed a significant increase of FAM1 and -2 intensities in edited events compared to the earlier experiments and a significant decrease in intensities in WT and mutated events. All samples were analyzed in quadruplicate. **(h)** Diamond box and whisker plot revealed the identification of all FAM signals visualized in the experiments and showed more signals remarkably measured in ExV than ExI, II, and-III; Error bars represent SE; Asterisks represent p-value as *≤0.05, **≤0.01, and ***≤0.001. **(i)** The bar plot represents the HDR efficiency in different experiments; The overlap data are shown as bin bars, and the standard distribution curves are added. HDR efficiency plot revealed that *XRCC4* deficiency (ExV) led to HDR happening significantly more than the fusion of CtIP (ExII), MRE11 (ExIII), and CtIP+MRE11 (ExV). Also, ExIV meaningfully revealed more HDR happening than ExII and -III.; Error bars represent SE; Asterisks represent p-value as **≤0.01, ***≤0.001, and ****≤0.0001; Triplicate technical repeats were considered for each sample.

Figure 5: Violin plots reveal the *BleoR* and *MKK2* expression and the success happening HDR via different experiments. **(a-e)** The differences between *BleoR* and *MKK2* expression. Three technical repeats were used for each event in this assay; Dash lines present quartiles; Solid lines present median. **(f)** Heat-map to show the effect of efficient HDR on the expression of NHEJ and HDR factors. Overexpression *CtIP* and/or *MRE11* caused to enhance the expression of *BRCA1*, *Rad50*, and *Rad51* and to demote the expression of *Lig4* and *XRCC4*. The highest expression of the HDR factors visualized in ExV means that *XRCC4* deficiency decreased the

879 expression of NHEJ factor *Lig4* and intensified HDR efficiency. Triplicate technical repeats were
880 considered for each sample.

881 **Figure 6:** Polymorphisms analysis. **(a)** Analyses of distributed indel nucleotides
882 happened on 5' and 3' homology arms and knocked in fragments throughout experiment
883 events. **(b)** Diamond box and whiskers for the mean comparisons of happened indel nucleotides
884 through experiment events. The exact numbers of indels are presented via the punching
885 column bars on the top-right corner. **(c)** Identification of the happened polymorphisms in
886 homology arms through the experiments. Box and Whisker plot revealed that most
887 polymorphisms happened in homology arms by ExI, and it was significantly more than those in
888 ExV and –IV; Asterisks represent p-value as *≤0.05; Error bars represent SE. **(d)** Stacked column
889 plot of total polymorphisms happened in DDT integration into the poplar genome. Insertions
890 and deletions were occurred much more than the other types. SNP and substitutions were
891 occurred less than the other types. Whisker and standard distribution curves exposed that the
892 total polymorphisms caused by *XRCC4* deficiency were less than the other experiments.

893 **Figure 7:** Radar diagrams of *MKK2* expressions, stem lengths, and -diameters from WT
894 and survived recovered events after NaCl treatment. No significant differences
895 in *MKK2* expressions and phenotypic changes before and after salt stress between WT and
896 survived recovered events confirmed the proper HDR.

897 **Supplementary data**

898 **Supplementary 1**: Schematic of pgRNA, DDT, and pDDT. **(a)** pgRNA included the *MKK2*
899 target seed and Cas9. **(b)** pDDT included DDT ligated into pRGEB31 by restriction enzyme
900 cloning method.

901 **Supplementary 2**: Schematic construction of DDT and pDDT fragments, primers, and
902 oligos.

903 **Supplementary 3:** Schematic construction of CtIP, MRE11, CtIP+MRE11, and XRCC4
904 cassette primers and oligos.

905 **Supplementary 4:** Schematic construction of cassettes (CtIP and MR) and vectors
906 (pgCtIP and pgMR) and their primers.

Supplementary 5 : Schematics of constructed cassettes and plasmids. **(a)** pgCtIP plasmid including CtIP cassette. **(b)** pgMR plasmid including MR cassette. **(c)** pgCtMR plasmid including CtMR cassette. **(d)** pggCtMR plasmid including XRCC4 cassette.

Supplementary 6: Schematic construction of cassettes (CtMR, XRCC4) and vectors (pgCtMR and pggCtMR) and their primers.

Supplementary 7: Alignment of events involved in experiment I.

Supplementary 8: Alignment of events involved in experiment II.

Supplementary 9: Alignment of events involved in experiment III.

Supplementary 10: Alignment of events involved in experiment IV.

Supplementary 11: Alignment of events involved in experiment V.

Supplementary 12: Schematic of TaqMan real-time PCR FAM and VIC target assays in this study. Yellow rectangles exhibited CDS.

Supplementary 13: Box-and-whisker (Min-Max) plots of one-dimensional FAM delta-delta Ct signals in designed experiments. All signals were calculated as quadruplicates.

Supplementary 14: Schematics of sequence analyzing of triggered events from different experiments. **(a)** Sequence analysis of triggered events included in EXII reveals one recovered event. **(b)** Sequence analysis of triggered events included in EXIII reveals one recovered event. **(c)** Sequence analysis of triggered events included in EXIV reveals four recovered events. **(d)** Sequence analysis of triggered events included in EXV reveals 12 recovered events.

Supplementary 15: The raw data of real-time PCR evaluates the percentage of delta-delta Ct mean from *BleoR* in all experiments. **(a)** Delta-delta Ct mean of *BleoR* expression from grown buds. Each sample was investigated with three technical repeats. **(b)** Descriptive statistic table of raw data calculated by ANOVA-One way.

Supplementary 16: Column plots of the expression of integrated *BleoR* and new recombinant *MKK2* genes via different designed experiments. Three technical repeats were used for each event in this assay; Error bars represent SD; WT and pDDT were used to control *MKK2* and *BleoR* expression, respectively.

Supplementary 17: Chromatogram alignments of events included in experiment V.

Supplementary Table

Supplementary Table 1: CRISPR sites located on 3' region of *MKK2*. The yellow highlight reveals the selected CRISPR target in this study.

Supplementary Table 2: Oligos and primers used in this study.

Supplementary Table 3: All polymorphisms detected in homology arms happened by HDR through experiments.

Supplementary Table 4: Variant nucleotides happened from experiments.

Supplementary Table 5: The raw data of RT-qPCR of *MKK2* expressions and phenotypic analyzes in WT and survived recovered events before and after salt stress. All events were analyzed in triplicates for RT-qPCR.

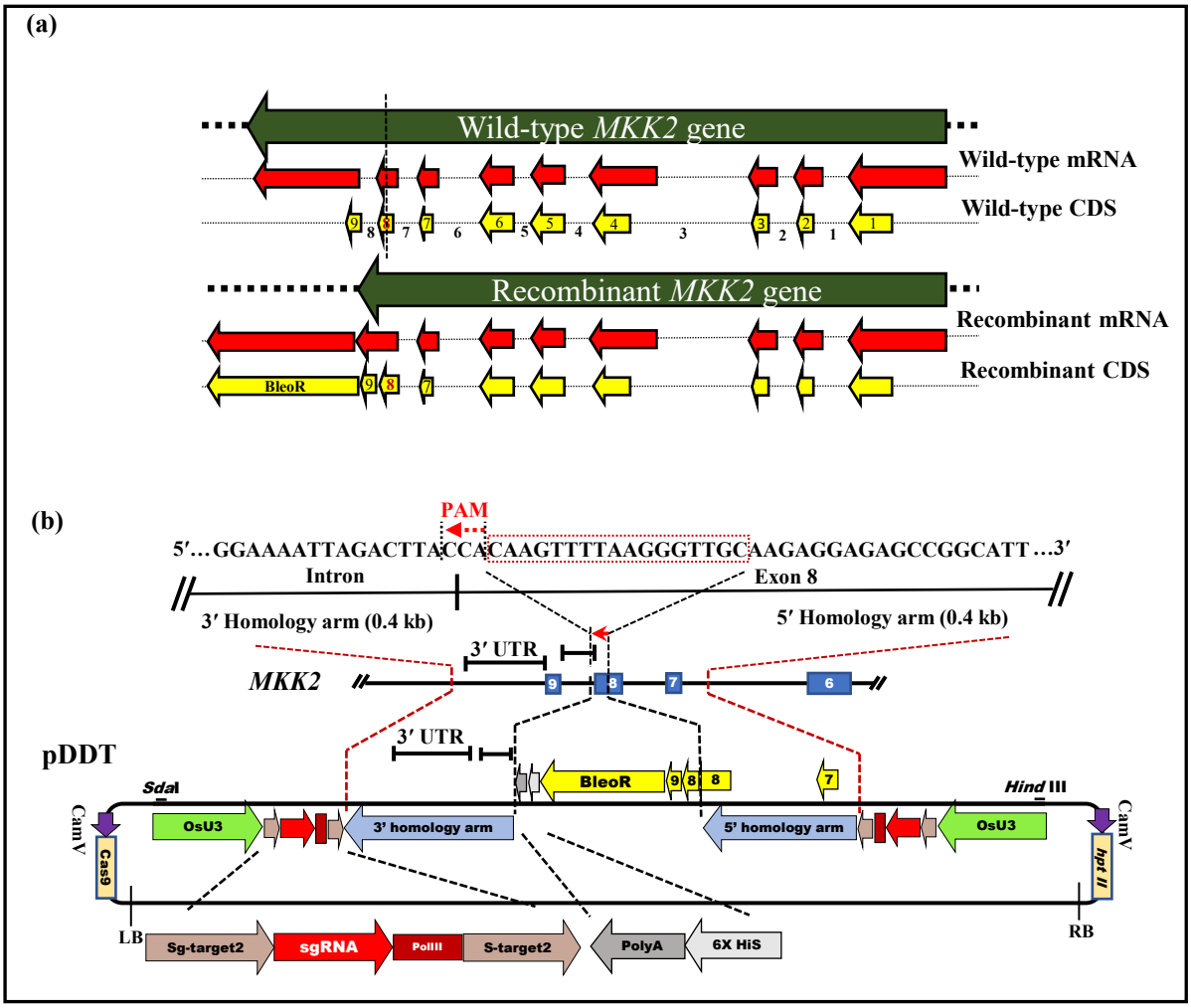

Figure 1: Schematics of *MKK2* locus before and after edition and integration of exogenous *BleoR* CDS into the poplar genome **(a)** Schematic of the purpose of this research to integrate exogenous BleoR into the poplar genome. Dash line reveals the target site. **(b)** Protospacer Adjacent Motif (PAM) was detected at the end of exon 8 to lead Cas9. 400 bp sequences from both sides of the CRISPR target were selected for HDR in this study. The 5' homology arm included part sequences of the intron between exon 6 and -7, exon 7, intron sequences between exon 7 and -8, and a part of exon 8. The 3' homology arm included intron sequences between exon 8 and -9 and 3' UTR of the *MKK2* locus up to 400 bp. Designed DDT included remained sequences of exon 8, exon 9, BleoR CDS, 6xHis, and PolyA sequences flanked by the 3'- and 5' homology arms. We added two special targets besides DDT. The DDT was then ligated into the pRGEB31 vector to form pDDT.

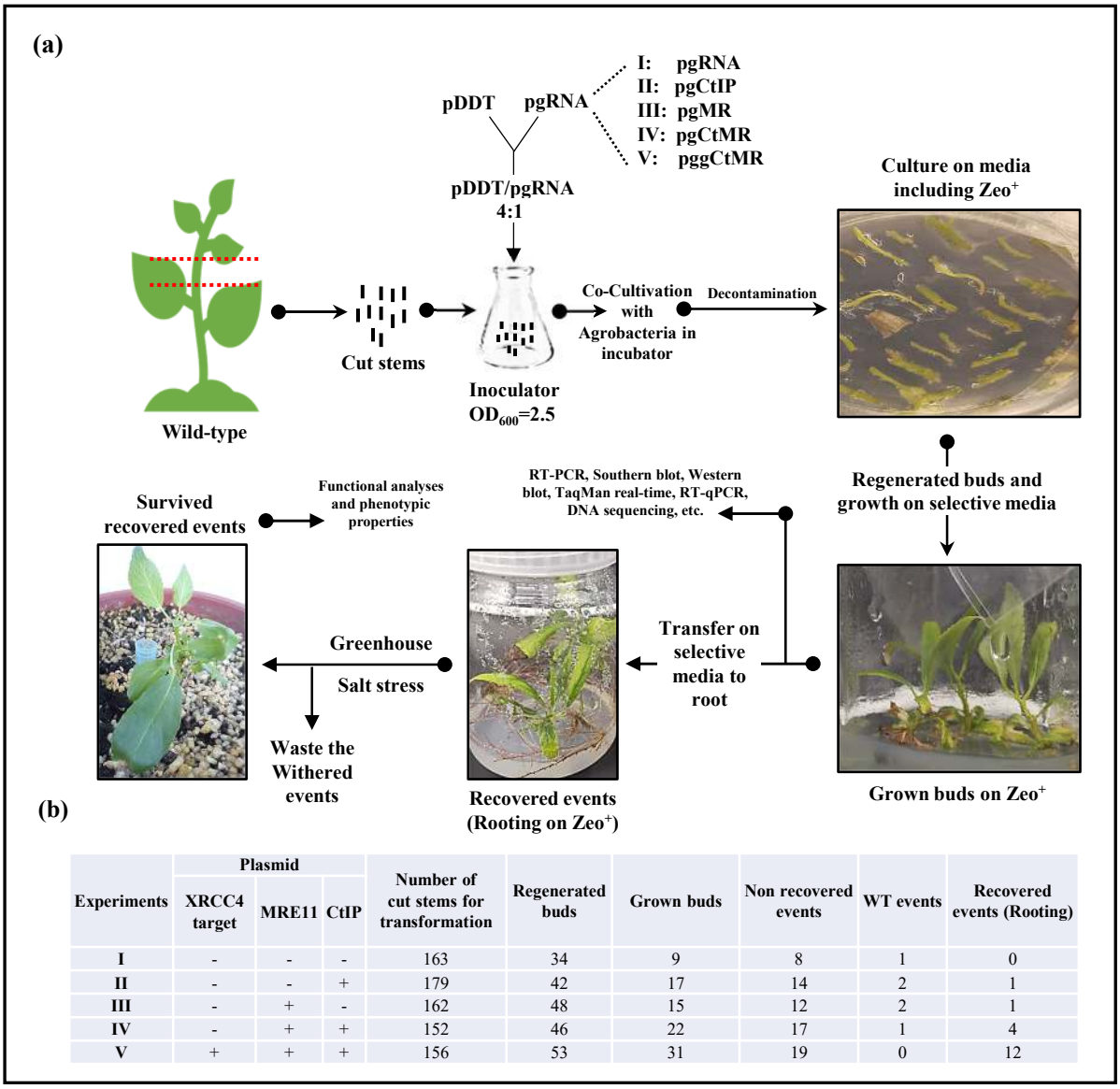

Experiments	Plasmid			Number of cut stems for transformation	Regenerated buds	Grown buds	Non recovered events	WT events	Recovered events (Rooting)
	XRCC4 target	MRE11	CtIP						
I	-	-	-	163	34	9	8	1	0
II	-	-	+	179	42	17	14	2	1
III	-	+	-	162	48	15	12	2	1
IV	-	+	+	152	46	22	17	1	4
V	+	+	+	156	53	31	19	0	12

Figure 2: The transformation strategy and designing of experiments. **(a)** pDDT and pgRNA were mixed 4:1 and introduced to the Agrobacterium tumefaciens to form inoculator suspension. We condensed inoculator up to OD600=2.5 and then dipped all cut off stems. The putatively edited events were regenerated on Zeocin. We allowed putative edited events to bud. The grown buds were then transferred on selective rooting media and allowed to be recovered. Recovered events were then planted on soil and following two weeks of acclimation introduced by salt stress **(b)** Designed experiments for this study including (I) No HDR factors, (II) overloaded CtIP, (III) overloaded MRE11, (IV) Overloaded CtIP+MRE11, and (V) Overloaded CtIP+MRE11 with *XRCC4* deficiency.

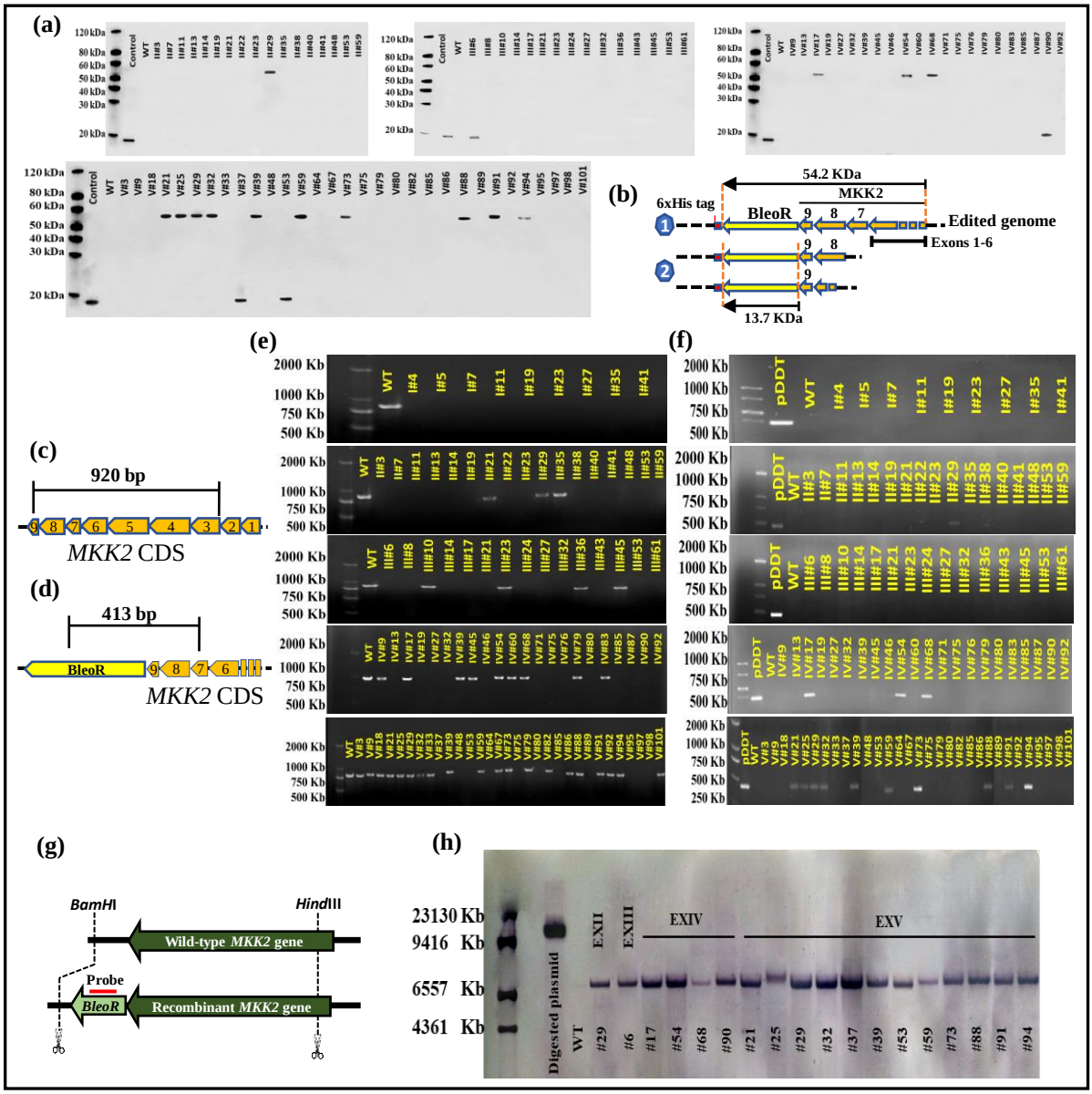

Figure 3: Western blotting to reveal the fused 6xHis tag with BleoR integration into the poplar genome. **(a)** Different experiments exhibited different quantities of 6xHis tag fusion. **(b)** Schematic of fusion 6xHis tag with edited poplar genome triggered by different experiments. Shape 1 reveals successful fusion of BleoR and MKK2 with about 54 kDa. Shape 2 reveals an unsuccessful combination of mentioned proteins with about 14 kDa. **(c)** Schematic of right HDR happening caused to attach exon 8 and 9 in the edited genome. **(d)** Schematic of proper integration in edited genome caused to connect the BleoR to the C-terminal of MKK2. **(e)** RT-PCR exhibited the HDR in exon 8 and 9, revealing a 920 bp of transcribed MKK2 RNA in triggered events from ExII to ExV. The β-actin was used as the control in all RT-PCR assays; WT was positive. **(f)** RT-PCR revealed that BleoR CDS was adequately inserted in the target region with amplifying 413 bp of transcribed RNA in the recovered events. The β-actin was used as the control in all RT-PCR assays; BleoR protein extracted from pDDT plasmid was used as the positive control. WT was used as the negative control. **(g)** Schematic of probing BleoR in edited events and WT as the control using Southern blotting. **(h)** Southern blot proved that BleoR CDS was integrated into the precise recombinant genome. Digested pDDT plasmid was used as the positive control.

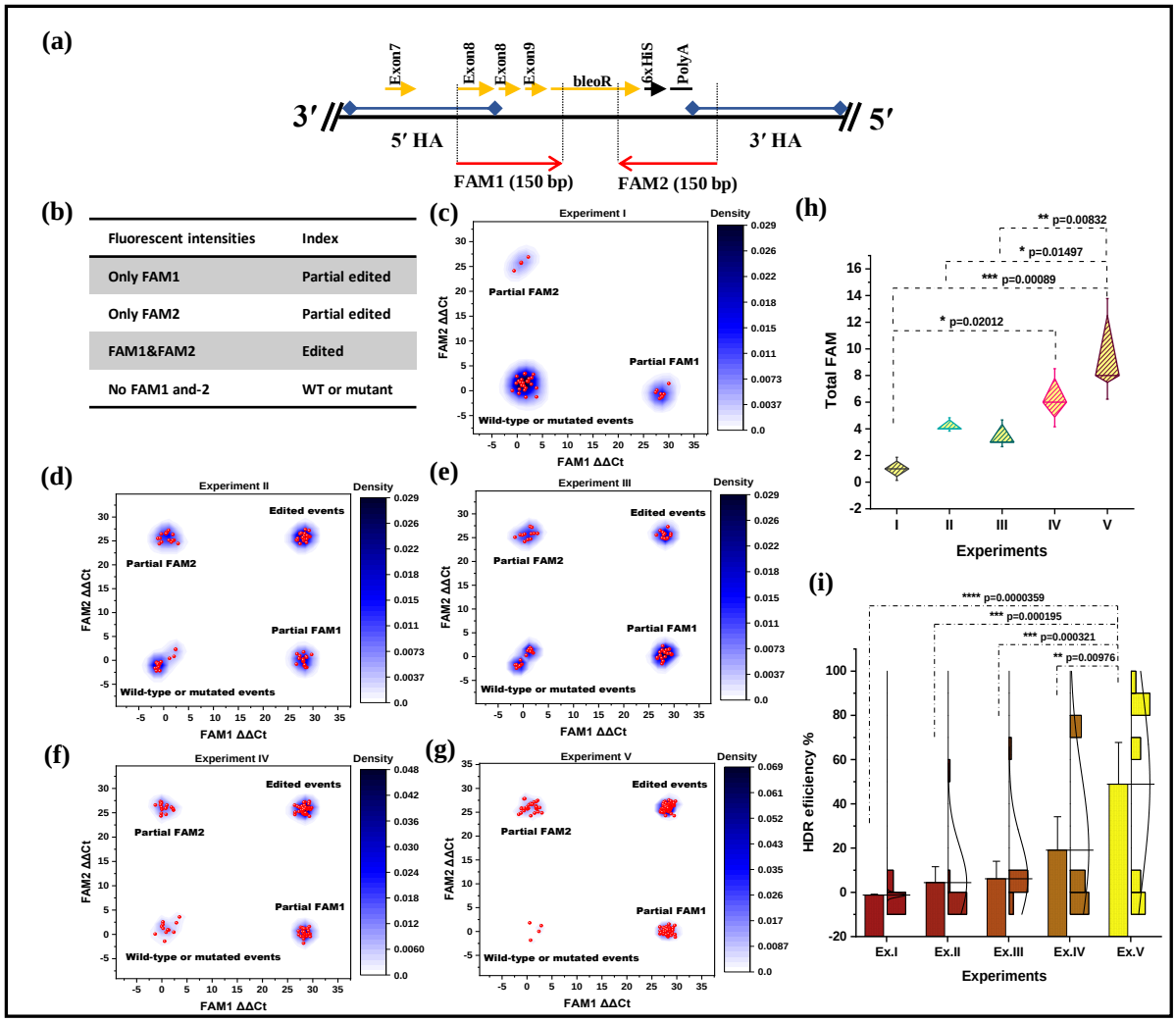

Figure 4: The 2D kernel density plot of TaqMan real-time PCR fluorescent intensities and HDR efficiency percentage. **(a)** The TaqMan real-time PCR assay designing to detect HDR happened, and evaluation included FAM1 and FAM2 DNA binding probes. **(b)** Strategy to classify edited events. **(c)** Experiment I revealed no density for the edited events. **(d)** The density plot of FAM1 and -2 intensities resulted from experiment II revealed an expansion in edited events against partial, mutant, and wild-types. **(e)** The density plot of FAM1 and -2 ΔΔCt resulted from experiment III revealed an increased intensity of partial FAM1 events. **(f)** Experiment IV revealed a remarkable increase of edited events signals in confronting with three earlier experiments. **(g)** The Density plot of experiment V revealed a significant increase of FAM1 and -2 intensities in edited events compared to the earlier experiments and a significant decrease in intensities in WT and mutated events. All samples were analyzed in quadruplicate. **(h)** Diamond box and whisker plot revealed the identification of all FAM signals visualized in the experiments and showed more signals remarkably measured in ExV than ExI, II, and-III; Error bars represent SE; Asterisks represent p-value as *≤0.05, **≤0.01, and ***≤0.001. **(i)** The bar plot represents the HDR efficiency in different experiments; The overlap data are shown as bin bars, and the standard distribution curves are added. HDR efficiency plot revealed that *XRCC4* deficiency (ExV) led to HDR happening significantly more than the fusion of CtIP (ExII), MRE11 (ExIII), and CtIP+MRE11 (ExV). Also, ExIV meaningfully revealed more HDR happening than ExII and -III.; Error bars represent SE; Asterisks represent p-value as **≤0.01, ***≤0.001, and ****≤0.0001; Triplicate technical repeats were considered for each sample.

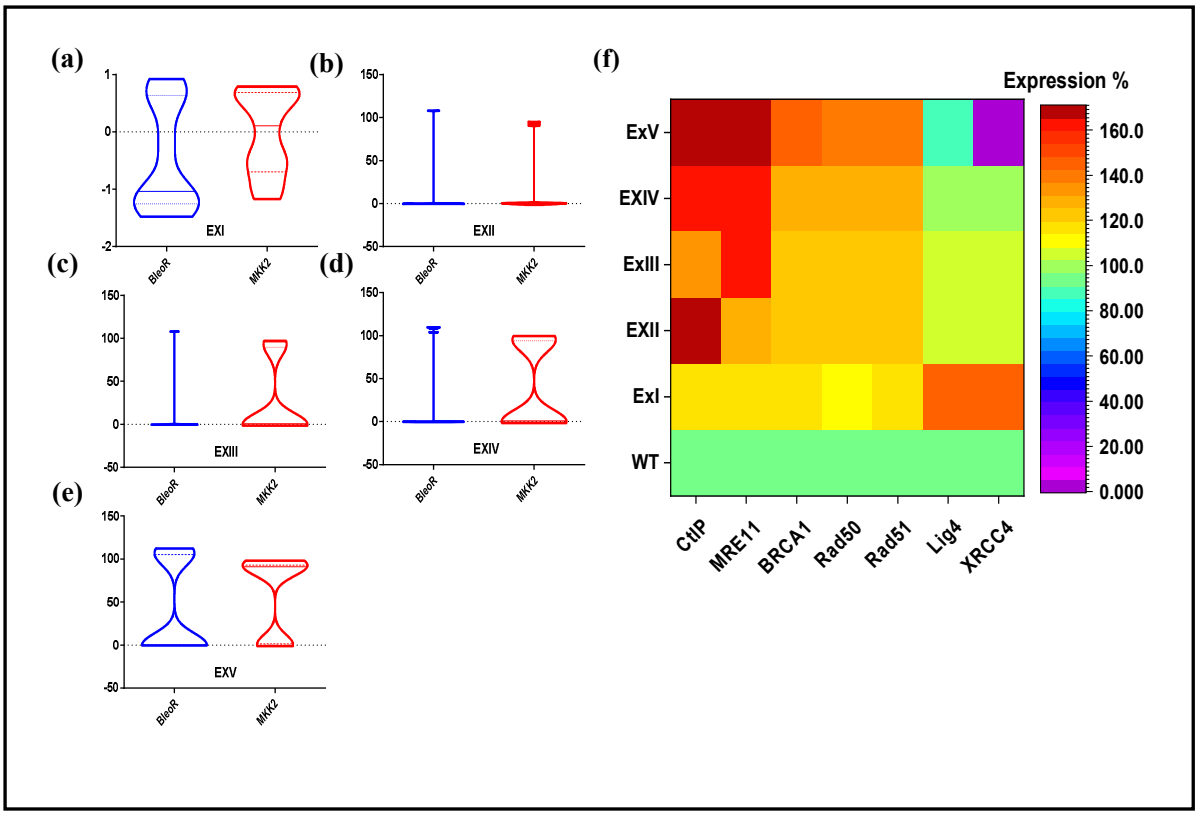

Figure 5: Violin plots reveal the *BleoR* and *MKK2* expression and the success happening HDR via different experiments. **(a-e)** The differences between *BleoR* and *MKK2* expression. Three technical repeats were used for each event in this assay; Dash lines present quartiles; Solid lines present median. **(f)** Heat-map to show the effect of efficient HDR on the expression of NHEJ and HDR factors. Overexpression *CtIP* and/or *MRE11* caused to enhance the expression of *BRCA1*, *Rad50*, and *Rad51* and to demote the expression of *Lig4* and *XRCC4*. The highest expression of the HDR factors visualized in ExV means that *XRCC4* deficiency decreased the expression of NHEJ factor *Lig4* and intensified HDR efficiency. Triplicate technical repeats were considered for each sample.

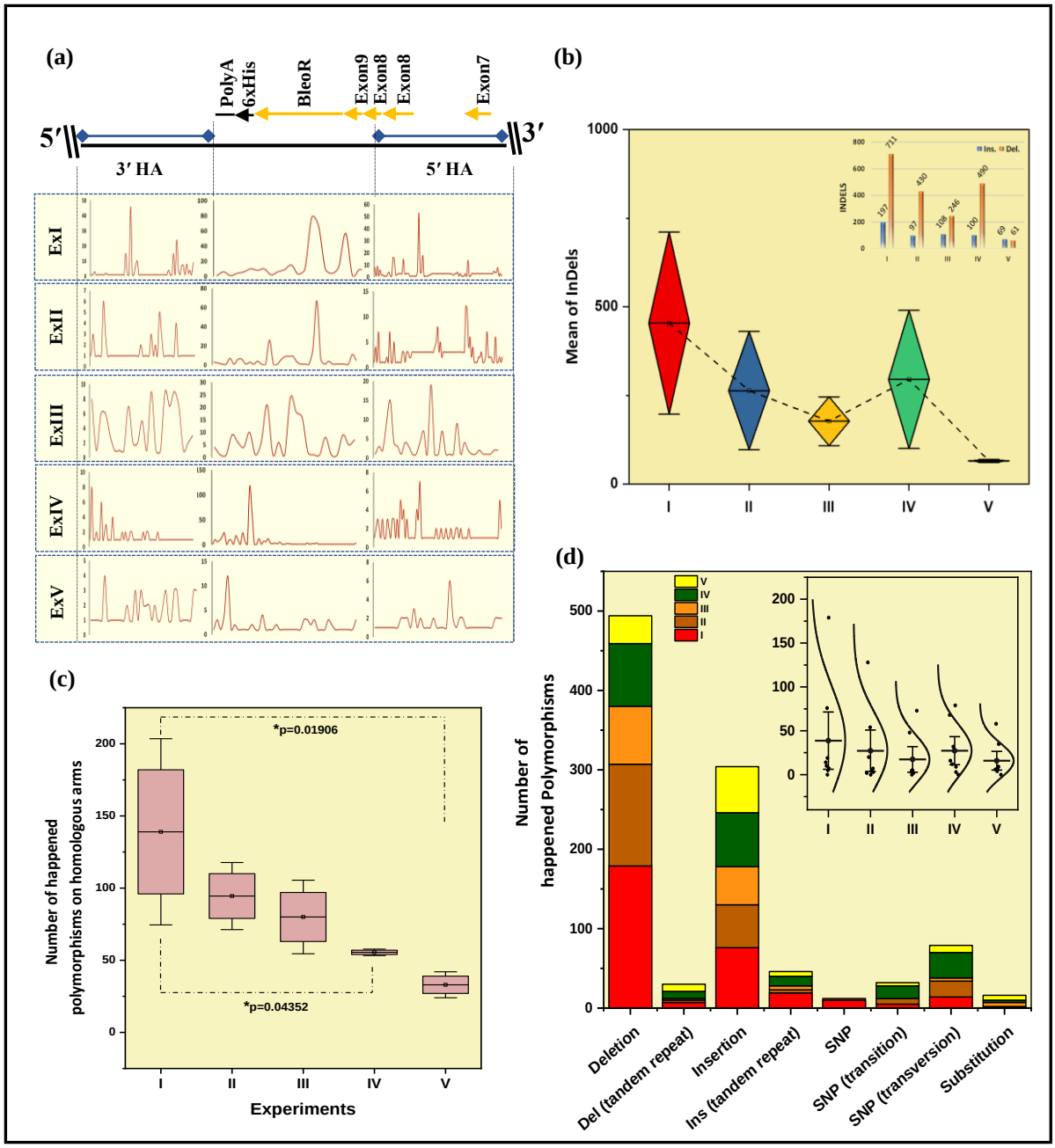

Figure 6: Polymorphisms analysis. **(a)** Analyses of distributed indel nucleotides happened on 5' and 3' homology arms and knocked in fragments throughout experiment events. **(b)** Diamond box and whiskers for the mean comparisons of happened indel nucleotides through experiment events. The exact numbers of indels are presented via the punching column bars on the top-right corner. **(c)** Identification of the happened polymorphisms in homology arms through the experiments. Box and Whisker plot revealed that most polymorphisms happened in homology arms by ExI, and it was significantly more than those in ExV and –IV; Asterisks represent p-value as *≤0.05; Error bars represent SE. **(d)** Stacked column plot of total polymorphisms happened in DDT integration into the poplar genome. Insertions and deletions were occurred much more than the other types. SNP and substitutions were occurred less than the other types. Whisker and standard distribution curves exposed that the total polymorphisms caused by XRCC4 deficiency were less than the other experiments.

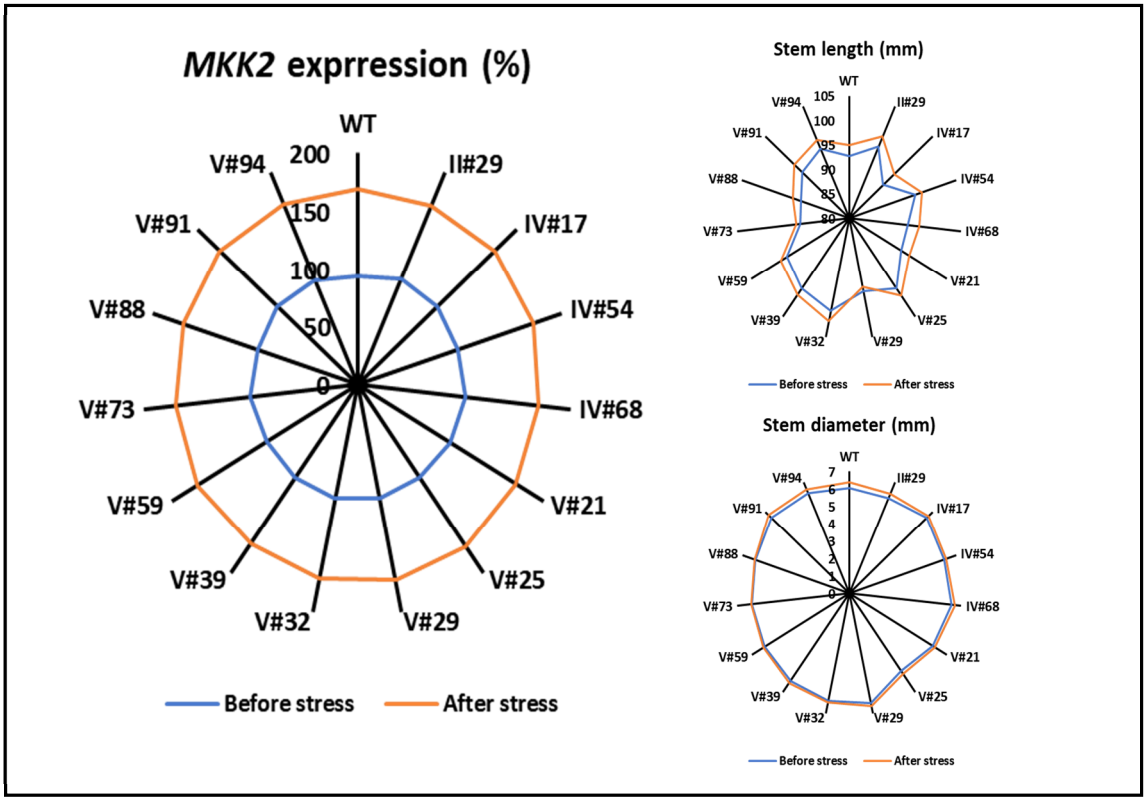

Figure 7: Radar diagrams of *MKK2* expressions, stem lengths, and -diameters from WT and survived recovered events after NaCl treatment. No significant differences in *MKK2* expressions and phenotypic changes before and after salt stress between WT and survived recovered events confirmed the proper HDR.